Journal of Building Engineering 63 (2023) 105409

Contents lists available at ScienceDirect

Journal of Building Engineering

journal homepage: www.elsevier.com/locate/jobe

Full length article

Mix optimization of hybrid steel and polypropylene fiber-reinforced concrete for anti-thermal spalling

Lei Shen [a,*], Xiupeng Yao [b], Giovanni Di Luzio [c], Mingkai Jiang [d], Yang Han [b]

[a] Hohai University, College of Water Conservancy and Hydropower Engineering, Nanjing, 210098, China
[b] Henan University of Technology, School of Civil Engineering, Zhengzhou, 450001, China
[c] Politecnico di Milano, Department of Civil and Environmental Engineering, Milan, 20133, Italy
[d] Henan Provincial Academy of Building Research, Zhengzhou, 450053, China

ARTICLE INFO

Keywords:
Pore pressure
Residual strength
High temperature
Hybrid fiber-reinforced concrete
Mix optimization

ABSTRACT

Concrete tends to spall explosively under fire due to the combined effect of thermal stress and pore pressure build-up. For an anti-spalling strategy in the concrete mix design, one can add steel fibers to improve the material strength and fine-polypropylene (PP) fibers to mitigate the pore pressure build-up. However, the addition of steel fibers causes noticeable increments in the spalling risk, while the addition of PP fibers causes slight decrements in the material strength capacity. Hence, the mix optimization of hybrid fiber reinforced concrete (HFRC) is studied in this research focusing on the individual and synergistic effects of steel and PP fibers on the mechanical degradations and pore pressure peaks at elevated temperatures. An apparent plateau in the pore pressure rises at 165 °C (PP melting point) is frequently observed in HFRC, which is the combined opposite effects of the two different fiber types. The increase of PP fiber length, rather than the dosage, is recommended to mitigate the pore pressure build-up, because of the better retention of residual strength and improvement in pore connection thanks to the observed fiber adhering effect (FAE) on aggregates. Based on a comprehensive experimental investigation, the cementitious mix with 1% of steel and 0.2% of 19-mm-length PP fiber in volume is recommended to obtain a high strength capacity and low pore pressure at elevated temperature. Finally, a new mathematical formula for prediction of the maximum pore pressure variation when steel, PP, or both fibers are employed in the concrete mix is here proposed for guiding the anti-spalling mix design of fiber-reinforced cementitious material.

1. Introduction

The thermal spalling of cementitious materials when it is exposed to elevated temperatures is known to be the combined result of two mechanisms: the produced thermal stresses and the pore pressure build-up [1–6]. Generally, the restricted thermal dilation generates a biaxial state of stresses with compressive stresses parallel to the heated surface and tensile stresses perpendicular to the heated surface [7,8]. Simultaneously, the pore pressure builds up, which is a consequence of the vaporization of water (free, physically and chemically bounded) in the cement paste at high temperature, also generates tensile stresses in the heated area [9,10]. To avoid thermal spalling, those two mechanisms must be controlled and/or limited [1,2,11,12].

From the viewpoint of thermal stress mechanism, the anti-spalling solution is to increase the material strength and/or to reduce the thermal stress during heating. Particularly, a widely accepted approach is to add steel fibers with high melting point into concrete

* Corresponding author.
E-mail address: shenl@hhu.edu.cn (L. Shen).

https://doi.org/10.1016/j.jobe.2022.105409
Received 8 August 2022; Received in revised form 30 September 2022; Accepted 12 October 2022
Available online 21 October 2022

because they can provide remarkable bridging forces in cracked material at ambient and high temperature (up to 800 °C) [13–15]. Moreover, the addition of steel fiber increases the thermal conductivity of steel fiber-reinforced concrete (SFRC) [13,16–18], resulting in a relative low temperature gradient with a reduced level of thermal stresses during heating. For those reasons the SFRC is believed to have a better fire resistance performance than the plain cementitious material. However, based on some experimental observations by Shen et al. [15], Biolzi et al. [19], Cattaneo and Biolzi [20] and Li et al. [11,21], the thermal spalling risk of SFRC is even higher than that of plain cementitious material. A possible explanation is the increase of the pore pressure build-up in the presence of steel fibers during heating. This can be due to the higher tensile strength of the material that produces a high-pressure of water vapor that cannot be released via crack propagations. For instance, Shen et al. [4], Lo Monte et al. [22] and Algourdin et al. [23] reported the occurrences of thermal spalling and the apparent pore pressure growth due to steel fiber addition in composites, when it is subjected both to a standard fire load (ISO-834) and a heating load with 10 °C/min up to 250 °C. Hence, a thorough investigation on the effect of different steel fiber dosages on the pore pressure development in concrete is needed to quantifies this effect in order to properly design the composites mix.

From the viewpoint of pore pressure mechanism, the anti-spalling solution is to reduce and, possibly, to suppress the pore pressure build-up in concrete during heating. In the past decades, it was experimentally proven that the addition of fine synthetic fibers can effectively prevent the pore pressure build-up because of a number of different mechanisms, which include the deformation of the fiber and the rupture of the weak fiber–matrix interfaces to accommodate expanding vapor as well as continuous tunnel-type voids for moisture migration [10,12,24–32]. Thanks to the pore pressure reduction, the spalling risk of fine synthetic fiber-reinforced concrete is much lower than that of plain cementitious material [12,28,29,33,34]. However, the formation of tunnel-type voids is a kind of thermo-chemical damage which leads to a deterioration of the concrete mechanical properties for temperatures above the melting temperature of the synthetic fibers [24,35].

Based on the above overview of the state-of-art, an anti-spalling mixture design would provide for the addition of both high-melting-temperature fibers to mitigate the thermal stress mechanism and low-melting-temperature fibers to alleviate the pore pressure mechanism. To be more specific, one can add steel fibers to increase concrete mechanical strength capacity and, at the same time, add fine synthetic fibers to suppress the pore pressure build-up during heating. In recent years, many researchers [11,14,18,21,26,27,36–38] explored the feasibility of this approach and started to investigate the multi-physical performances of the hybrid steel-fine synthetic fiber-reinforced concrete at/after high temperature exposure.

Bangi et al. [26,27] performed experimental investigations on the effect of fiber type and their geometry on the pore pressure development in high strength concrete at elevated temperatures. Two important findings were reported in these works: (1) regarding the pore pressure suppression, the polypropylene (PP) fibers works better than the polyvinyl alcohol (PVA) fibers. Hence, the fine PP fibers are adopted as the low-melting-point fibers in the present work. (2) The increase of dosage and length of fine PP fiber produces a decreasing effect on the pore pressure build-up. This result suggests the need of in-depth investigation on the development of pore pressure in order to optimize dosage and geometry of the fibers to be used. Algourdin et al. [23] reported a reduction of the maximum pore pressure at a depth of 60 mm from the heated surface from 2.9 bar to 1.4 bar due to the presence of PP fibers (V_f = 0.082%). In recent years, the research group of Prof. Tan [11,14,21,30,36–38] conducted many experiments on the pore pressure development and the explosive spalling risk of hybrid steel-PP fiber-reinforced cementitious materials exposed to high temperature. They showed that the combined use of PP and steel fibers increased at high temperature the material permeability because of the melting of PP fiber and the micro-crack network caused by thermal cracks between steel fibers/aggregates and matrix, and thus preventing the explosive spalling. However, in those studies the pore pressure developments of plain cementitious material and SFRC were not entirely recorded due to explosive spalling.

These aforementioned studies demonstrated the effectiveness of pore pressure lowering in hybrid steel-fine PP fiber-reinforced concrete (HFRC) when exposed at high temperatures. However, there is still a lack of a systematic and quantitative research on the pore pressure evolution that considers the combined effect of different types of fibers. This is needed for a proper design of composites mixes with a minimum spalling risk and for the calibration and validation of multi-physics numerical models [4,5,39–43]. To meet this need, in this research a series of experimental tests on the individual and synergistic effects of the fine PP fiber dosage and length, and the steel fiber dosage on the pore pressure development in concrete subjected to a fast-heating load with moderate target temperature (500 °C) is performed and their results are hereafter presented.

2. Experimental procedure

2.1. Materials and mix proportions

In the experimental campaign, thirteen different cementitious mixes are considered: one plain cementitious material, as the reference mixture, and twelve fiber-reinforced concrete as listed in Table 1. All these mixes have the same components: ordinary Portland cement 42.5, polycarboxylate superplasticizer as admixture, river sand with diameter 0.25 mm–3.5 mm, and crushed limestone with maximum diameter of 25 mm. For fiber-reinforced mixes, the commercially available fibers, namely hooked-end steel fibers and monofilament polypropylene fibers, are used, which meet the requirements of the Chinese technical specification for fiber-reinforced concrete structures (CECS 38:2004) [44]. The fine PP and steel fibers employed in the mixes are shown in Fig. 1. The steel fibers are 30 mm in length and 0.55 mm in diameter, with a melting temperature of 1500 °C. The nonabsorbent polypropylene fibers with a melting temperature of 165 °C have an equivalent diameter of 48 μm with three different lengths: 6 mm, 12 mm, and 19 mm.

Table 1
Composition of concrete mixtures (Unit: kg/m^3).

Mix	Cement	Water	Fine Agg.	Coarse Agg.	Superplast.	Steel fiber	PP fiber
S0P0	500	150	713	1027	13.5	0	0
S1P0	500	150	713	1000	13.5	79	0
S2P0	500	150	713	973	13.5	156	0
S0P2L12	500	150	713	1027	13.5	0	1.82
S0P4L12	500	150	713	1027	13.5	0	3.64
S0P2L6	500	150	713	1027	13.5	0	1.82
S0P2L19	500	150	713	1027	13.5	0	1.82
S1P2L12	500	150	713	1000	13.5	79	1.82
S1P4L12	500	150	713	1000	13.5	79	3.64
S2P2L12	500	150	713	973	13.5	156	1.82
S2P4L12	500	150	713	973	13.5	156	3.64
S1P2L6	500	150	713	1000	13.5	79	1.82
S1P2L19	500	150	713	1000	13.5	79	1.82

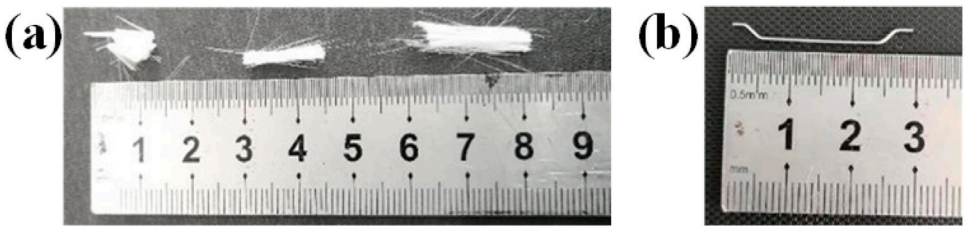

Fig. 1. Adopted fibers: (a) fine PP fibers; (b) steel fibers.

For the sake of conciseness and clarity, all mixes are labeled based on their fiber type, fiber length, fiber dosage, and specimen number. Therefore, the label "S*n*" denotes steel fibers addition with a volume fraction of *n* in % (*n* = 0%,1%,2%), "P*n*" denotes PP fibers with a volume fraction of *n* in ‰ (*n* = 0‰,2‰,4‰), "L*x*" denotes the *x* mm length of the PP fibers, and "-*m*" (*m* = 1,2) denotes the specimen number since two tests are performed for each mix. For example, S1P2L12-2 stands for the second specimen with 1% of steel fiber volume fraction and 0.2% volume fraction of fine PP fibers with a 12 mm length. After casting, these specimens of 200 mm × 200 mm × 100 mm are kept in the mold for 24 h and then cured under standard condition in a climate room (with relative humidity>95% and temperature of 20 ± 2 °C) for 28 days.

2.2. Experimental setup

The setup of the experimental test is shown in Fig. 2. Thermal load is applied on the bottom of the composites specimen by means of a computer-controlled radiant heater placed 50 mm below it. The furnace has a heating power of 1500 W and is able to reach a maximum temperature of 1500 °C. In the experiments, the furnace temperature increases to the maximum temperature of 500 °C within 10 min, and then the maximum temperature is maintained for three hours. In the next one hour, the specimen is kept in the furnace to cool it down naturally. The fast heating rate of 50 °C/min is here adopted to mimic the thermal shock of ISO 834 fire curve, and the target temperature of 500 °C is designed. It is important to remark that this research work aims to provide quantitative guidance for concrete mix against spalling, thus an optimization study needs objective data. In this regard, the qualitative observations of spalling cannot be adopted as the optimization objective in this study. Hence, the primary objective of this study is to obtain the minimum of pore pressure peak values (being one of the main cause of spalling) and, at the same time, to obtain the maximum of compressive strengths. However, the pre-tests with the original target temperatures of 600 °C showed spalling with the resulting test quit and failure. For this reason, the target temperature is reduced to 500 °C in order to avoid explosive thermal spalling, so that the full pore pressure and temperature evaluations can be recorded as the objective optimizing data. The lateral faces of the specimens are thermally insulated using firebricks with asbestos to enforce unidirectional heat propagation in each of them.

All specimens are instrumented with pressure gauges to measure the evolutions of pore pressure under thermal loading. Three gauges are placed in the central zone of each specimen at a distance of 20 mm, 40 mm and 60 mm from the heated side, see Fig. 2. The gauges [9,26,45,46] are made of a metal tube with inner diameter of 4 mm and a metal cup encapsulated by a disk of porous sintered metal (ϕ14 mm × 4 mm). The metal tube is welded to a metal cup at one end and is screwed to a metal tee-junction at the other end. The metal tee-junction connects to a pressure transducer with measurement range of 0 MPa-8 MPa and accuracy of 0.01 kPa. A metal end cap is used to seal the gauge that is filled with a thermostable silicone oil. In addition, K-type thermocouples, having a covering of glass fibers, are attached to the gauges for measuring temperature inside the heated specimens. A syringe needle with a length of 700 mm is used to fill the gauges with the oil from the cap end continuously, to ensure that no air bubbles are trapped inside the gauge. After an accurate assembly of pressure gauges and thermocouples, they are in turn connected to the data logger before the test. The authors want to remark that such experiments [3,9,10,12,21,26–29,33,45] are significant for a better

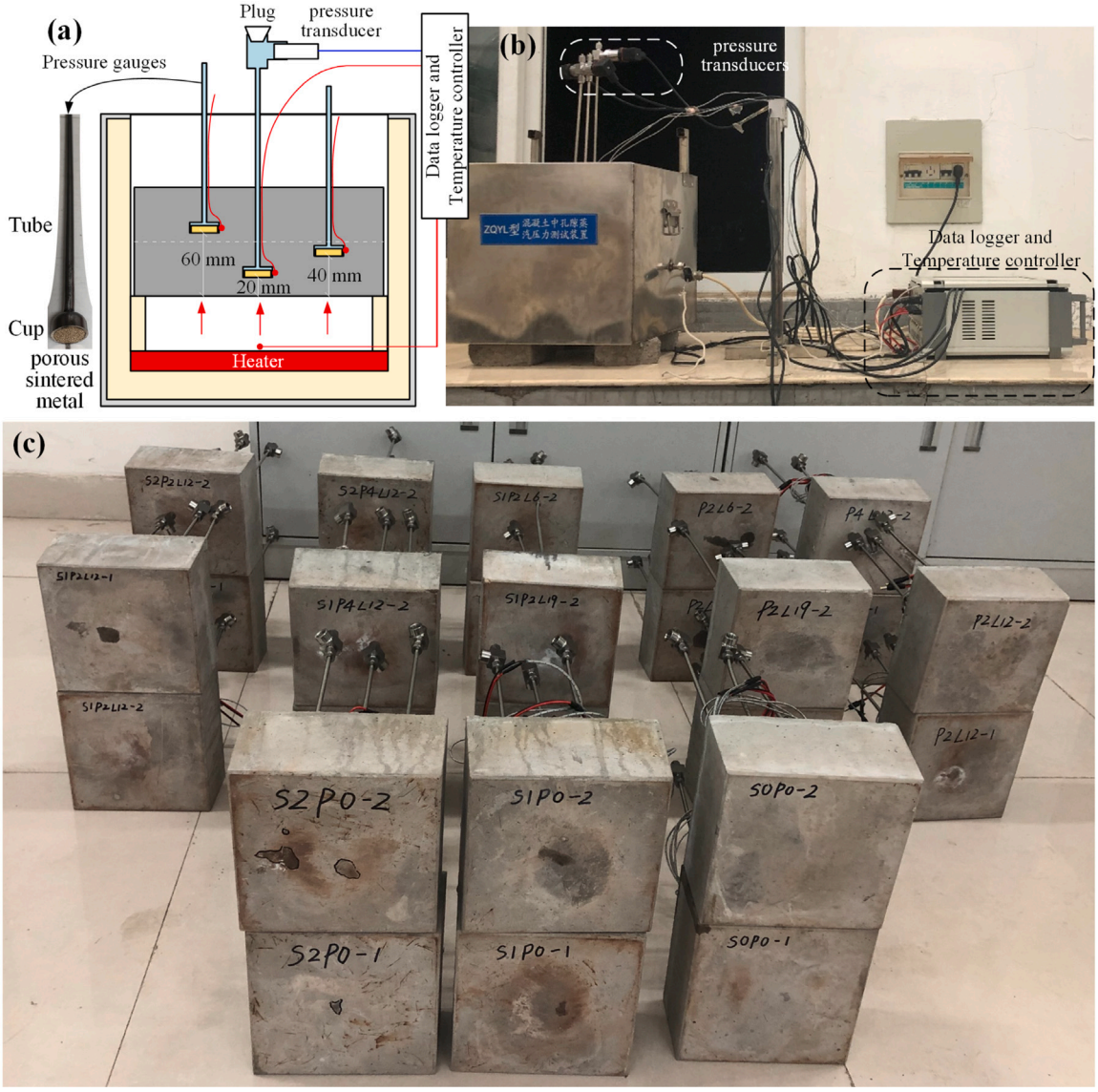

Fig. 2. Experimental setup: (a) sketch of the pressure gauges in the specimens; (b) data acquisition system; (c) overview of the specimens after the thermal loading tests.

understanding of the thermo-hygro coupled behavior inside a cementitious composite during heating and can provide unique data that are needed to develop numerical models [4,5,39–42], although the pressure gauges may not capture the pore pressure induced by the liquid phase [5,47].

In addition to the pore pressure tests, uniaxial compression, thermal conductivity and porosity tests on most of the mixes have been performed before and after the preheating treatment. The preheating treatment includes a heating with a rate of 5 °C/min up to the target temperature of 600 °C, then 3 h at target temperature, and after that a natural cooling stage in the furnace. All the specimens reach a uniform distribution of the target temperature at the end of the five-hour preheating phase [48,49]. In the mechanical test, an electro-hydraulic servo testing machine with load range of 0–5000 kN and load accuracy of 1% is used. The load rate of 0.3 MPa/s and no-friction medium between the specimen and loading platens is applied. Six specimens for each mix are heated up to 600 °C to avoid the influence of the possible spalling. The compression strength is the average of three compression strengths within the range of ±10% their average strength [44].

In the thermal conductivity test, the transient plane source (TPS) method via the equipment of Hot Disk DZDR-S (Nanjing, China) is employed which covers the measurement range from 0.005 W/(m °C) to 300 W/(m °C). Also the porosity tests have been conducted based on the ASTM cold-water saturation technique [50]. These specimens are heated in the oven at 60 °C and 600 °C to

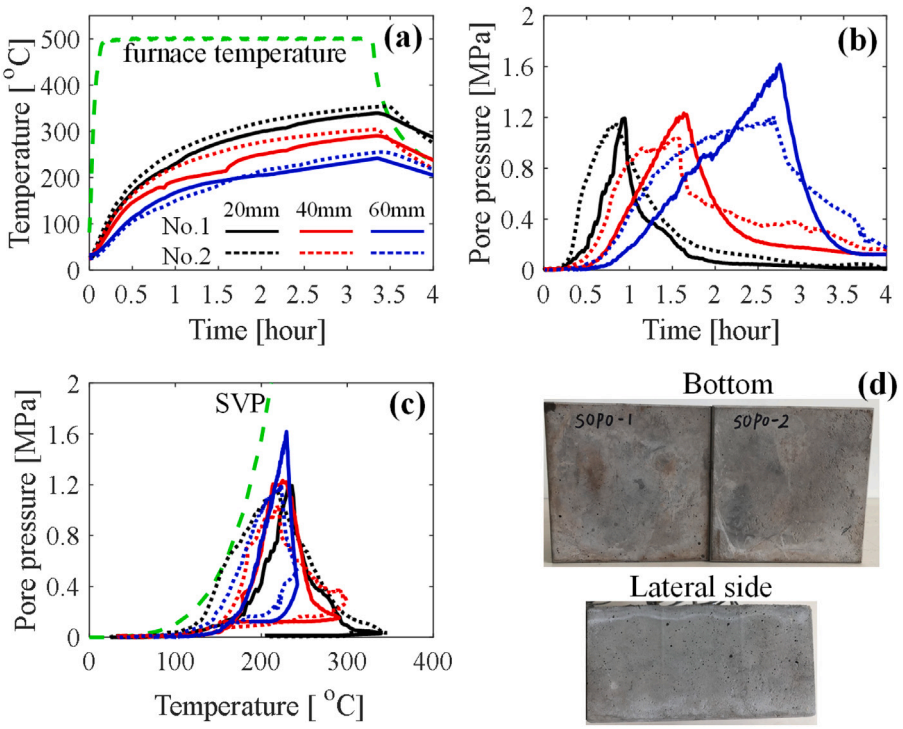

Fig. 3. Temperatures and pore pressures measured in S0P0: (a) temperature vs. time; (b) pore pressure vs. time; (a) pore pressure vs. temperature; (d) specimens after the thermal loading.

determine the oven-dry mass (W_d), and then immersed in water at approximately 20 °C for 72 h to determine the saturated surface-dry mass (W_s) and buoyant mass (W_b), respectively. The permeable porosity of cementitious composites can be calculated based on the weight gain due to water absorption and weight loss because of buoyancy, which can be written as $(W_s - W_d)/(W_s - W_b) \times 100\%$.

3. Results

3.1. General observations

The temperature and pore pressure measurements over time during the heating process inside the plain cementitious material (S0P0) are reported in Fig. 3 as the reference data. Consistently with the literature [9,45], the temperature evolves with a monotonically increase during heating, on the contrary, the pore pressure evolutions present the typical unimodal distribution shape. The pore pressure peak values at various depths are in the range between 1.0 MPa and 1.6 MPa, among which the maximum is observed at the depth of 60 mm in S0P0-2. The pore pressure peak values recorded in the present work is relatively lower than those reported in literature. This is mainly caused by the low target temperature (500 °C) which has been precautionary selected to avoid explosive spalling in the tests. Fig. 3(c) shows the relationships between pore pressure and temperature measured at the three different depths. These relationships have similar trend especially in the increasing phase and they never exceed the Saturated Vapor Pressure (SVP) [4,39,51,52]. The curves of S0P0-1 rise faster and closer to SVP but they reach lower pore pressure peaks then those of the second specimen, S0P2-2. All the pressure peaks occur in the temperature range between 200 °C and 230 °C, and afterward the pore pressure drops to a lower level. This phenomenon can be explained as follows. The pore pressure evolution (moisture migration) is strongly related to the temperature, and its build-up is mainly induced by the pore water evaporation. Once the pore pressure grows up, the pore water migrates to low-pressure area driven by the pressure gradient. An amount of water mass is transported to the high temperature area and escapes especially from the heating side through the thermal cracks (and tunnel cracks if fiber with low melting point is added). Another amount of water mass migrates in the opposite direction with lower temperature. This part of water vapor condensates to liquid water forming the so-called "moisture clog". Accompanied by the condensation, the pore pressure dramatically drops down. When the moisture clog moves to the cold side, the liquid water leaks from the cracks can be observed.

Exposure of concrete to high temperatures may cause considerable variations in the mechanical properties with irreversible loss of strength and stiffness, and increased ductility in the post-peak regime [4,40,48,49,53]. The results of the uniaxial compression tests on cube (100 mm × 100 mm × 100 mm) and the thermal conductivity tests with and without heating treatment are reported in Table 2. The controlled plain cementitious material (S0P0) exhibits a cubic compression strength of 70.2 MPa at room temperature

Table 2
Compression strength, thermal conductivity and porosity of the studied mixes.

Temp. treatment	Compression strength [MPa]		Thermal conductivity W/(m °C)		Porosity [%]	
	Before	After	Before	After	Before	After
S0P0	70.2	40.8	1.78	0.97	1.50	17.29
S1P0	90.2	45.6	1.88	1.04	2.05	17.91
S2P0	95.2	51.6	2.02	1.02	2.37	26.37
S0P2L6	69.1	39.4	1.76	0.88	2.00	16.42
S0P2L12	69.4	34.2	1.77	0.89	1.67	16.36
S0P2L19	69.5	34.5	1.75	0.88	1.82	15.85
S1P2L6	95.6	52.2	1.89	0.93	1.64	15.80
S1P2L12	95.0	47.4	1.89	0.98	1.53	16.71
S1P2L19	89.1	49.8	1.90	1.01	1.60	15.91

which conforms the design value of 60 MPa. After the high-temperature treatment, the uniaxial compression strength reduces up to 40.8 MPa. The addition of steel fibers enhances the mechanical strength of the SFRC before and after heating treatment; conversely the PFRC mixes show no variation of the compressive strength compared to that of plain cementitious material before heating, whereas a strength reduction after heating. As expected, the HFRC mixes present a remarkable increase in the uniaxial compression strength before and after the heating treatment. It is interesting to mention that, in the preheating treatment, 1/6 of plain concrete specimens, 1/6 of S1P0 specimens and 2/6 of S2P0 specimens showed explosive spalling, while all the other samples did not show any spalling. This circumstance confirms the righteousness of target temperature in the pore pressure test.

Regarding the thermal conductivity before the heating treatment, the addition of steel fibers causes an increase of the thermal conductivity; conversely, the addition of PP fibers slightly reduces it. After the thermal treatment, the thermal conductivity of all mixes experiences a significant reduction due to the thermal damage. These data corroborate the experimental evidence in the literature [13,14,16,38].

3.2. Effect of steel fibers

To study the influence of steel fiber content on the pore pressure rise inside the specimens, two different dosages of steel fibers, namely 1% (S1P0) and 2% (S2P0) of volume fraction, have been considered. Figs. 4 and 5 report the experimental measurements for S1P0 and S2P0, respectively. Consistently with the increase of the thermal conductivity (see Table 2), also the temperature rises with respect to time in SFRC mixes is slightly faster compared to the reference cementitious material, S0P0. Concerning the maximum pore pressure, the addition of steel fiber does cause a significant variation only for the volume fraction of 2%. As a matter of fact, the pore pressure peaks range from 0.6 MPa to 1.2 MPa for S1P0 and from 1.2 MPa to 1.7 MPa for S2P0. It is worth noting that the pore pressure of S2P0 at the depth of 20 mm in the No. 2 specimen losses the whole pressure raise over 0.6 MPa. This problem may be caused by the air trapped in the metal tee-junction connection. There could have been some air leaks from the threaded connections when the pressure of silicone oil reaches 0.6 MPa. Comparing the peak values of S0P0, S1P0 and S2P0, one can observe that by adding 1% volume fraction of steel fibers there is a tiny reduction of the pore pressure peak, on the contrary by adding 2% volume fraction of steel fibers a noticeable increment in pore pressure peaks is recorded.

The curves of pore pressure vs. temperature for S1P0 and S2P0 are reported in Figs. 4(c) and 5(c), respectively. It is apparent that the pore pressures closely raise along the SVP and partially exceed the SVP at the temperature range of 50 °C–150 °C. This phenomenon indeed reflects the migration of over-saturated water [5,47,54–56] which is also observed in other experiments [3,26–28]. Like S0P0, all pore pressure peaks present a value below the SVP in the temperature range of 200 °C–250 °C.

The observed results can be explained by considering that the influence of steel fibers on the pore pressure build-up in SFRC is twofold. The first effect is a release of the pore pressure which is induced by the additional thermal cracks, because a small crack volume increment can induce a plummet of pore pressure in its raising phase that is mainly produced by the mismatched rates of moisture migration and water vaporization [4,5]. The additional thermal cracks are caused by the higher thermal expansion coefficient of the steel fibers than that of matrix [57,58], as illustrated in Fig. 6. The second effect is an increase of the pore pressure which is attributed to the greater internal cohesion due to the fiber bridging-forces and the larger thermal energy attributed to the higher thermal conductivity, see Table 2. The higher thermal conductivity leads to faster temperature rises in the SFRC specimens, see Fig. 5(a). The higher absorbed thermal energy during heating means more energy for the latent heat of mass phase changes and for the vapor pressure. As a result, we observe higher and earlier pore pressure peaks than those of plain cementitious material, as illustrated in Figs. 4 and 5. Interestingly, based on the present experimental results, the decreasing effect is dominant in S1P0 with small steel fiber content (1%), whereas the increasing effect becomes dominant in S2P0 with a higher fiber content (2%).

3.3. Effect of PP fibers

To study the influence of fine PP fiber content on the pore pressure rise during heating inside the specimen, two different dosages of PP fibers with a length of 12 mm, namely 0.2% (S0P2L12) and 0.4% (S0P4L12) volume fraction, are tested. Figs. 7 and 8 present the experimental measurements for S0P2L12 and S0P4L12, respectively. The addition of PP fibers shows a negligible influence on the temperature rise, but a significant impact on the pore pressure build-up during heating. As can be observed in Figs. 7(b) and

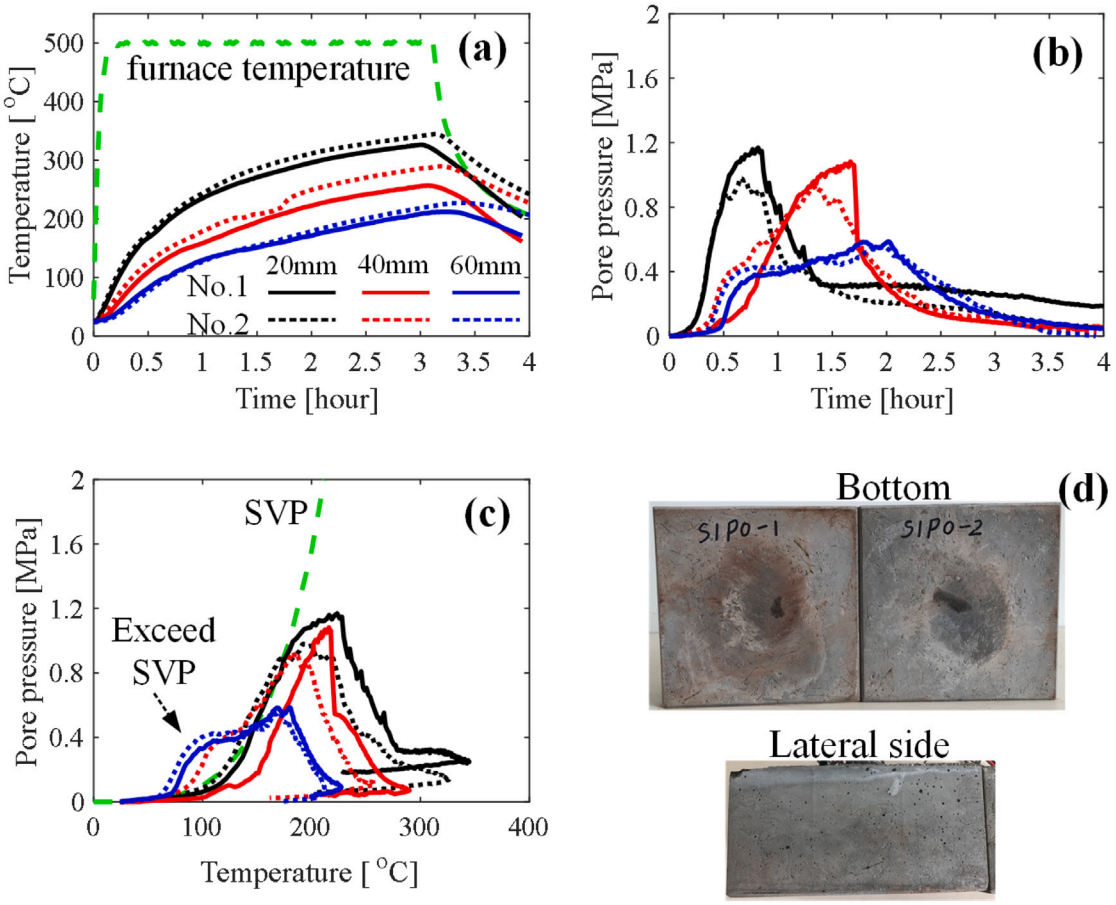

Fig. 4. Temperatures and pore pressures measured in S1P0: (a) temperature vs. time; (b) pore pressure vs. time; (a) pore pressure vs. temperature; (d) specimens after the thermal loading. (For interpretation of the references to color in this figure legend, the reader is referred to the web version of this article.)

8(b), the values of pore pressure peak range between 0.4 MPa and 0.8 MPa for S0P2L12 and between 0.2 MPa and 0.5 MPa for S0P4L12, showing that the larger the PP fiber dosage the greater the reduction of the maximum pore pressure. Note that for the specimen S0P2L12-2 the position of one gauge (expected at 20 mm) is closer to heated side and, consequently, an early pore pressure peak is displayed. Also, in specimen S0P4L12-2 the pore pressure data at an expected depth of 60 mm is actually at a real position of 40 mm depth as it can be estimated from the corresponding temperature data (see the blue dashed curve in Fig. 8).

The plots of pore pressure vs. temperature for S0P2L12 and S0P4L12 are reported in Figs. 7(c) and 8(c), respectively. One can observe that the increase of PP fiber dosage engenders a reduction of the pore pressure and its growing rate for the same temperature, which never exceeds the SVP. As in the previous results on plain cementitious material and SFRC, all the pore pressure peaks take place in a temperature range of 180 °C–250 °C.

The significant reduction of the pore pressure build-up recorded in this study due to the presence of fine PP fibers is in line with the literature results [10,12,27–29]. The pore pressure relief mechanism can be mainly attributed to the melting and evaporation of PP fibers during heating. At temperature up to 100 °C, the PP fibers have a negligible influence on the water mass transport. The PP fiber endothermic melting phase starts at 150 °C, reaches a peak at 165 °C and fully completes at 176 °C. The melting process of PP fibers destroys their crystallinity to create a wholly amorphous polymer [24,35]. Generally, the damage of the weak fiber–matrix interface takes place under raising pore pressure which let the vapor migrate in this space created by the rupture of the poor interfacial contact. This process has been termed as the pressure-induced tangential space (PITS) [24,28,30,35] and it allows steam to travel along this space even before the melting of the fiber. According to our view, this is the most relevant mechanism that reduces the pore pressure peaks, also because the PITS increases the pore connectivity. Increasing the temperature, the PP fiber vaporization takes place at a temperature of 325 °C with a maximum of the vaporization at about 460 °C that completes at 475 °C. This vaporization consists of an endothermic pyrolysis that involves the break-up of the carbon backbone into smaller molecules [24,35]. After this process, the tunnel-type voids appear at the positions of fine PP fibers, i.e. spaces vacated by vaporization of the PP fibers, that creates continuous channels for moisture-vapor migration especially in connection to thermal cracks [24,35]; see dash labels in Fig. 9. This results in a significant increment of permeability at high temperature in all mixes containing PP fibers [37], which improves the water mass transport capability so that the pore pressure raising rate and the pressure peak reduce during heating.

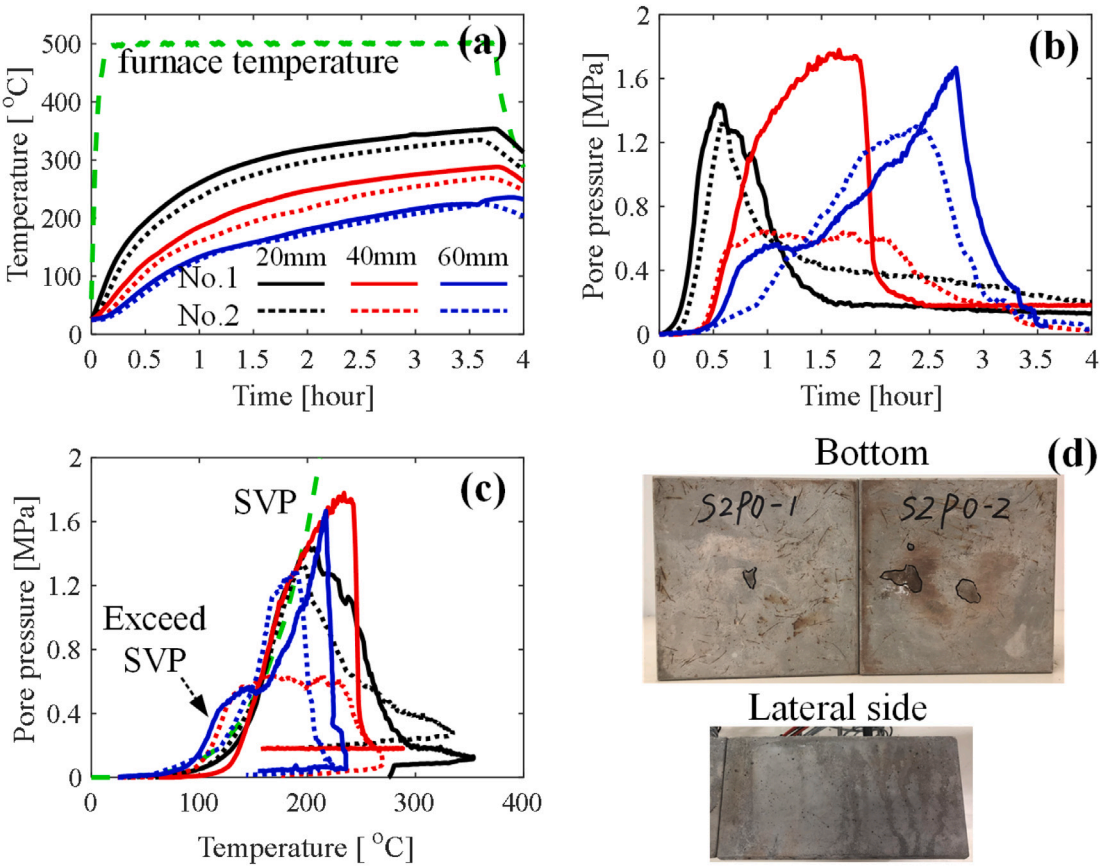

Fig. 5. Temperatures and pore pressures measured in S2P0: (a) temperature vs. time; (b) pore pressure vs. time; (a) pore pressure vs. temperature; (d) specimens after the thermal loading.

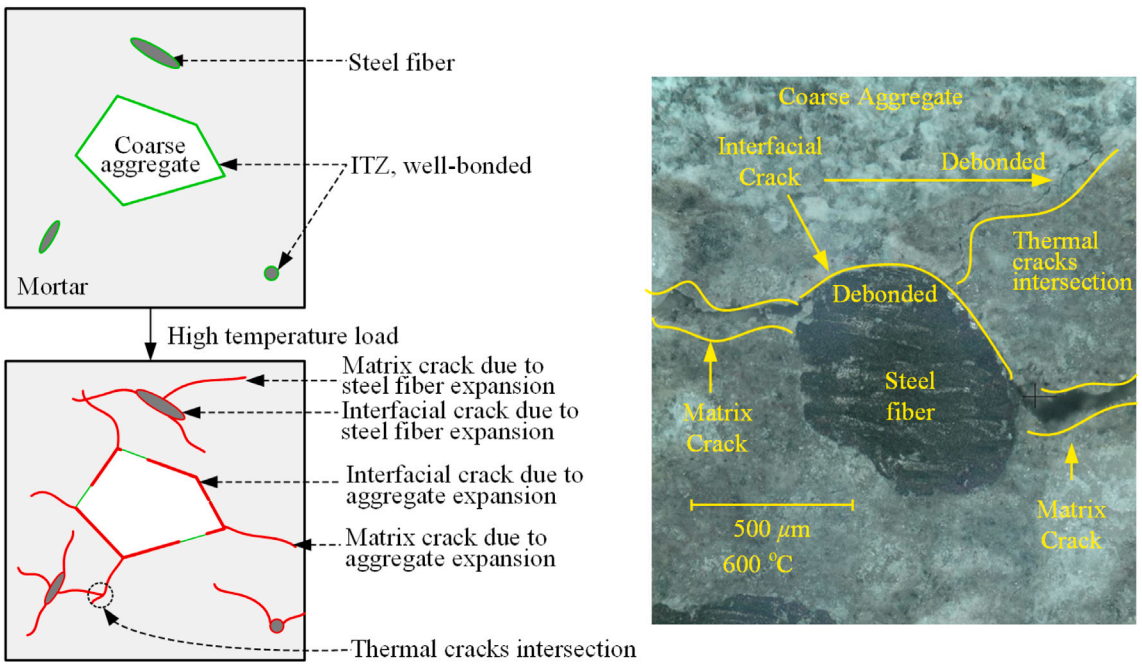

Fig. 6. Illustration of the thermal damage in SFRC.

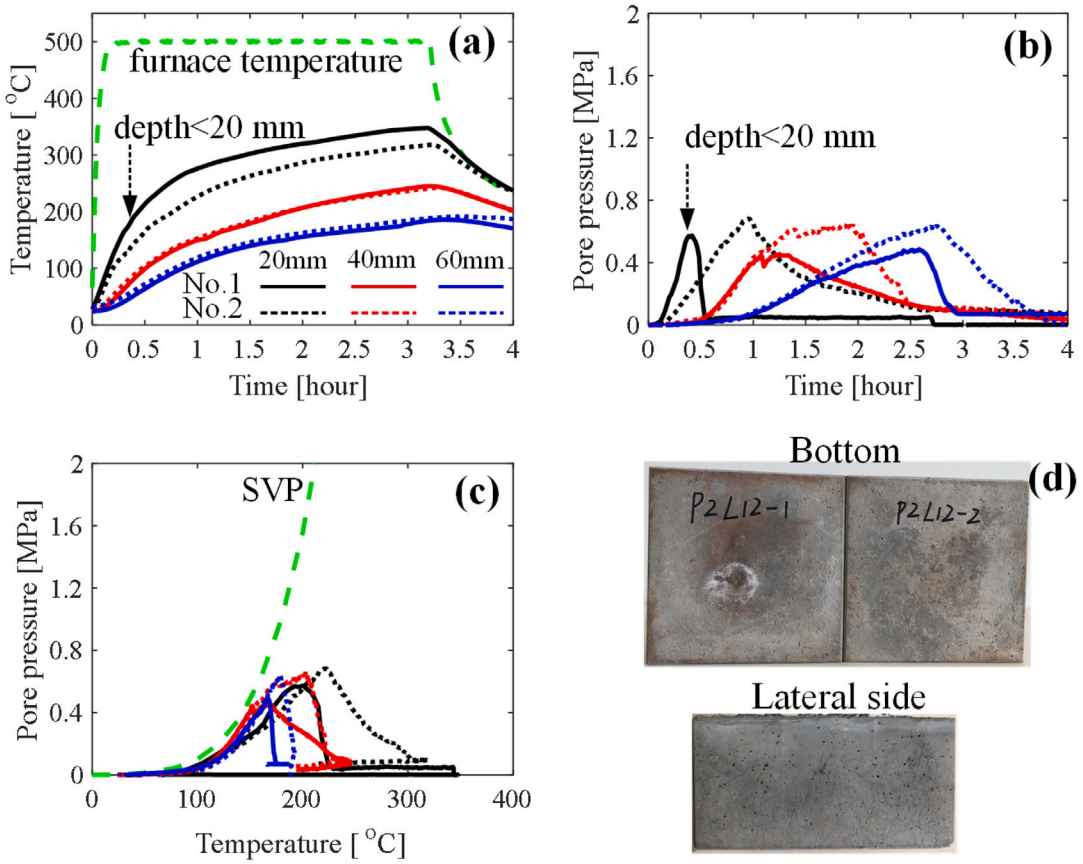

Fig. 7. Temperatures and pore pressures measured in S0P2L12: (a) temperature vs. time; (b) pore pressure vs. time; (a) pore pressure vs. temperature; (d) specimens after the thermal loading.

In addition to that, as revealed by the images from the scanning electron microscope (SEM) shown in Fig. 9, the soft fine PP fibers can partially adhere especially on the external surface of coarse aggregates. This circumstance leads to an increase of permeability in a region which is more porous in itself and damaged firstly by the effect of thermal action. This phenomenon is here called *fiber adhering effect* (FAE) and it is caused by the fact that the PP fiber diameter (48 μm) is close to the thickness of interfacial transitional zone (ITZ) [59–61]. In this case the pressure reduction mechanisms, described above, occur in the ITZ increasing the interfacial effect between matrix and coarse aggregates that in turn enlarges the pore connectivity of the fibers themselves. As a result, the FAE amplifies the PP fiber effect of reducing the pore pressure build-up becoming more effective. The FAE was also speculated by Kalifa et al. [10] but only here it is clearly observed via SEM images.

It should be noted that the pore pressure peak typically occurs in the temperature range of 150 °C–250 °C (see Figs. 3, 4, and 5) that is before the of PP fiber vaporization (pyrolysis). This means that the pressure reduction mechanisms, such as the PITS in combination with the FAE, are the most effective since they operate within the temperature range from 100 °C to about 250 °C.

3.4. Effect of PP fiber length

To study the influence of fine PP fiber length on pore pressure development during heating inside the samples, different PFRC mixes containing a fixed content (0.2% volume fraction) of PP fibers with a varying length are tested. In Fig. 10 the measurements of the mix S0P2L6 with PP fibers of 6 mm length are reported, in which the pore pressure peak of 1.1 MPa is recorded in the first gauge, whereas in the others the pore pressure peak gradually decreases up to a minimum value of 0.8 MPa. In Fig. 11 the experimental results of the mix S0P2L19 with PP fiber of 19 mm length show that the pore pressure at each depth is between 0.2 MPa and 0.6 MPa. The results of the mix S0P2L12 with PP fibers of 12 mm length are reported in Fig. 7, which have been discussed in the previous section and present a pore pressure peaks in the range from 0.4 MPa to 0.8 MPa. Therefore, the comparison between the results of mixes S0P2L6, S0P2L12, and S0P2L19 clearly demonstrates that the increase in fine PP fiber length has a monotonic reducing effect on the pore pressure development, at any rate, for fixed volume fraction of 0.2%. This result shows that longer PP fibers are more effective in mitigating pressure rise inside cementitious composite compared to shorter ones. The relationship between the recorded pore pressure and temperature of the mixes S0P2L6, S0P2L12, and S0P2L19 is reported in Figs. 10(c), 7(c)

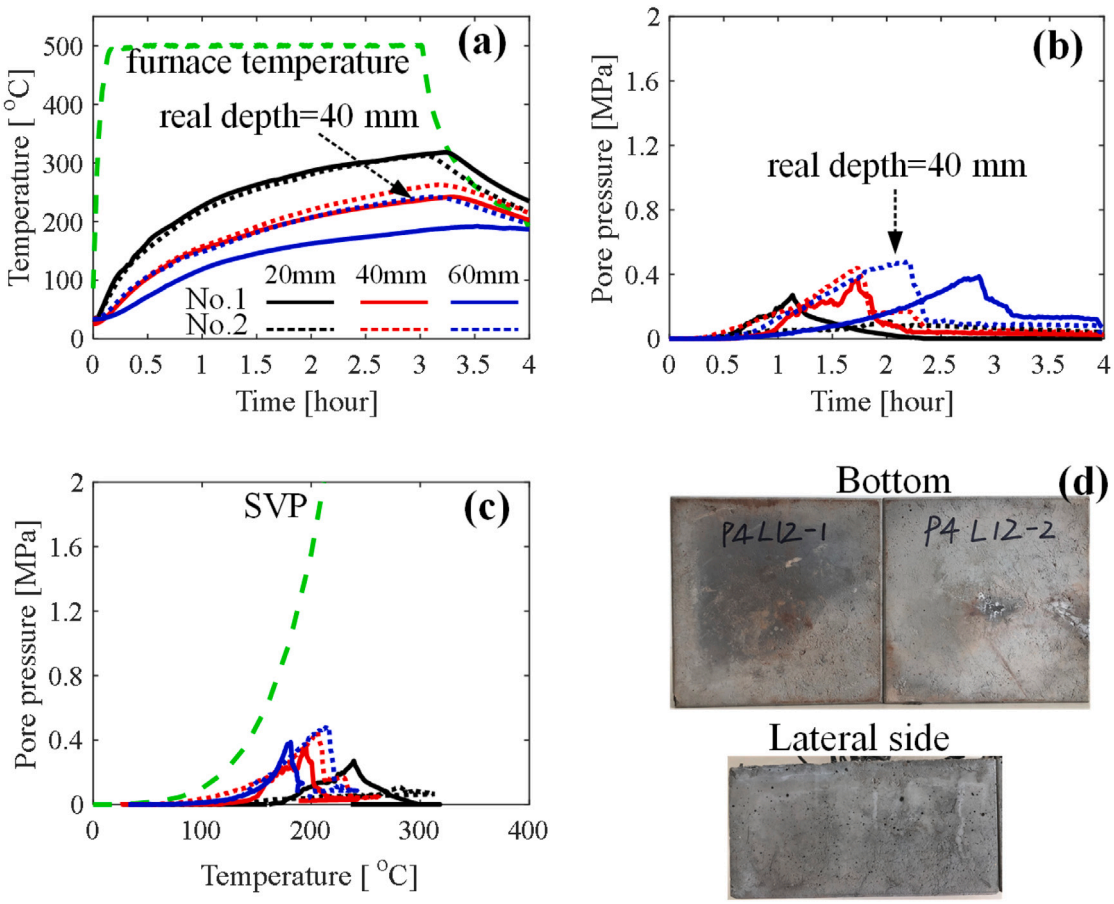

Fig. 8. Temperatures and pore pressures measured in S0P4L12: (a) temperature vs. time; (b) pore pressure vs. time; (a) pore pressure vs. temperature; (d) specimens after the thermal loading. (For interpretation of the references to color in this figure legend, the reader is referred to the web version of this article.)

and 11(c), respectively. The curves of the three PFRC mixes do not present a clear trend in the pore pressure rate with the increasing temperature for different lengths of the fibers, while the pore pressure value never exceed the SVP.

The observed experimental results presented in Figs. 7, 10, and 11 can be explained by the fact that the longer fibers can provide a larger interconnectivity of the porosity than the shorter ones during heating, although the increase of the overall porosity is the same having the mixes the same fiber content. This emphasizes the fact that the effective pore connectivity is much more important than the porosity itself and this is valid for all the transport processes in cementitious materials [62,63]. This deduction is supported by the porosity decrement with the increase of fiber length for PFRCs after the heating treatment, as reported in Table 2. The porosity decrements are mainly attributed to the better improvement of pore connectivity caused by longer PP fiber for temperatures above the material melting and vaporization point, so that more pore pressure is released and less pressure-induced cracks are generated. In addition, increasing the length of the PP fibers it is expected an increment of the number of fibers in contact with the aggregates in the ITZ magnifying the FAE mechanisms. This phenomenon was also commented by Kalifa et al. [10] as the probability of a fiber to touch two different aggregates which increases with the increment of the fiber length. Similar results were observed in the experiment investigations of Bangi et al. [26,27], in which they showed that the fine PP fiber with a double length work much better in the reduction of the pore pressure. The effects of the fiber geometry that directly affect the cumulative length and cumulative surface area of fibers, which in turn significantly affects the creation of reservoirs (micro-cracks) and continuous channels, were also reported in [64].

The selection of the optimal PP fiber length must also consider its influence on the mechanical strength, especially after the thermal loading. As reported in Table 2, the increase of fiber length causes slight reduction of the uniaxial compression strength after the heating treatments, since a better connectivity between pores and tunnel-type voids generated by the melted PP fibers also creates preferential paths for damage and cracks. Therefore, an optimal low-melting-point fiber length is required to be long enough to achieve a sufficient reduction in the pore pressure build-up, while at the same time the fibers should not be too long to affect the mechanical capacity of the composite too much.

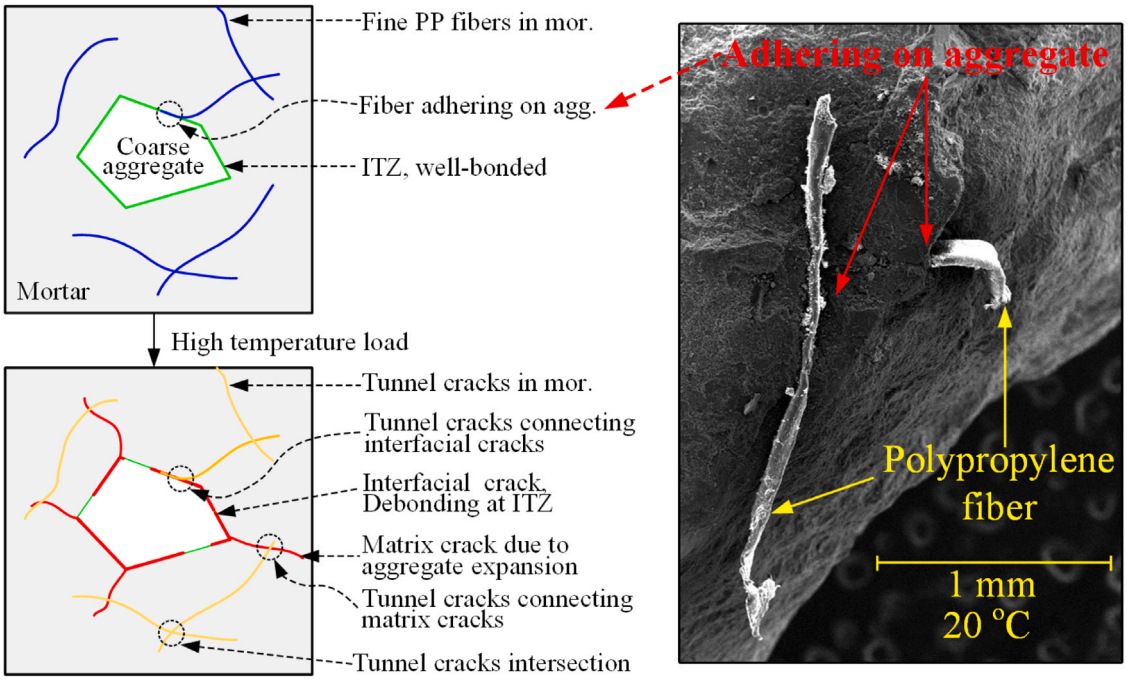

Fig. 9. Illustration of the thermal damage in PFRC.

3.5. *Synergistic effect of steel and PP fibers*

To study the synergistic influence of steel and fine PP fibers on pore pressure evolution during heating, four HFRC mixes with fixed PP fiber length (12 mm) are employed in this study. In Fig. 12 the results of the S1P2L12 mix containing 1% of steel fibers and 0.2% of PP fibers in volume are presented, in which the pore pressure reaches a maximum value of 1.15 MPa at the depth of 40 mm and 60 mm. In Fig. 13 the measurements of the S2P2L12 mix containing 2% of steel fiber and 0.2% of PP fiber in volume are reported showing a maximum value of the pore pressure of 1.2 MPa at 40 mm only for the specimen S2P2L12-2, while the other peaks are between 0.7 MPa and 0.8 MPa at other depths. In Fig. 14 the experimental data of the S1P4L12 mix containing 1% of steel fiber and 0.4% of PP fiber in volume present a pore pressure at each depth that is below 0.65 MPa. Finally, in Fig. 15 the experimental measurements of S2P4L12 mix containing 2% of steel fiber and 0.4% of PP fiber in volume are plotted with the peaks of the pore pressure that gradually increase with the depth and reach a maximum of 0.71 MPa at 60 mm depth.

The influence of steel fiber addition on the pore pressure rise can be observed by comparing the experimental results of the mixes S0P2L12, S1P2L12 and S2P2L12, S0P4L12, S1P4L12 and S2P4L12 with each other. As explained in Section 3.2, the addition of steel fiber has twofold effect on pore pressure development: a reduction due to the produced damage and cracks that induce its release; an increase that is attributed to the internal cohesion enhancement and the thermal conductivity increment. As observed in the experimental results, the increasing effect of steel fiber on pore pressure build-up is visible for S1P2L12 and S2P2L12, but the increasing effect is only marginal for S1P4L12 and S2P4L12. This difference implies that the increasing effect of steel fibers on the pore pressure can be effectively weakened by increasing the dosage of PP fiber. The influence of the addition of PP fibers on the pore pressure rise can be observed by comparing the results of the mixes S1P0, S1P2L12 and S1P4L12, S2P0, S2P2L12 and S2P4L12 with each other. As discussed in Section 3.3 and Section 3.4, the decreasing effect of PP fibers is remarkable in the mixes thanks to the growth of pore volume and connectivity principally due to the PITS and the FAE. The mechanism of the synergistic effect of the two types of fibers on pore pressure build-up is illustrated in Fig. 16. Steel fibers with higher thermal expansion coefficient cause additional thermal cracks in the matrix [11,36] that add to the PITS and FAE mechanisms of the PP fibers. As a result, there is an increase of the porosity and its connectivity, especially at the interface of both coarse aggregates and steel fibers.

By comparing the results of the four HFRC mixes (Figs. 12, 13, 14, and 15) with those of the reference plain cementitious material (Fig. 3) and SFRC (Figs. 4 and 5), one can infer that the pore pressure peaks in HFRC mixes are effectively suppressed below 0.7 MPa by the addition of PP fibers. At the same time, the residual compression strength of HFRC is improved by the presence of steel fibers (see Table 2). In another word, the HFRC mixes make up for the shortcomings and inherit the advantages of the mixes with just one type of fiber. The present results demonstrate that the HFRC is a material that owns a very low spalling risk since the two different types of fibers act on both mechanisms that causes the explosive spalling: the pore pressure build-up and the thermal stresses.

It is noteworthy that pore pressure plateaus in the HFRC are often observed at the PP fiber melting temperature during the heating process. For example, as highlighted in the Figs. 12(b), 13(b), and 15(b), the pore pressure evolution shows an apparent plateau

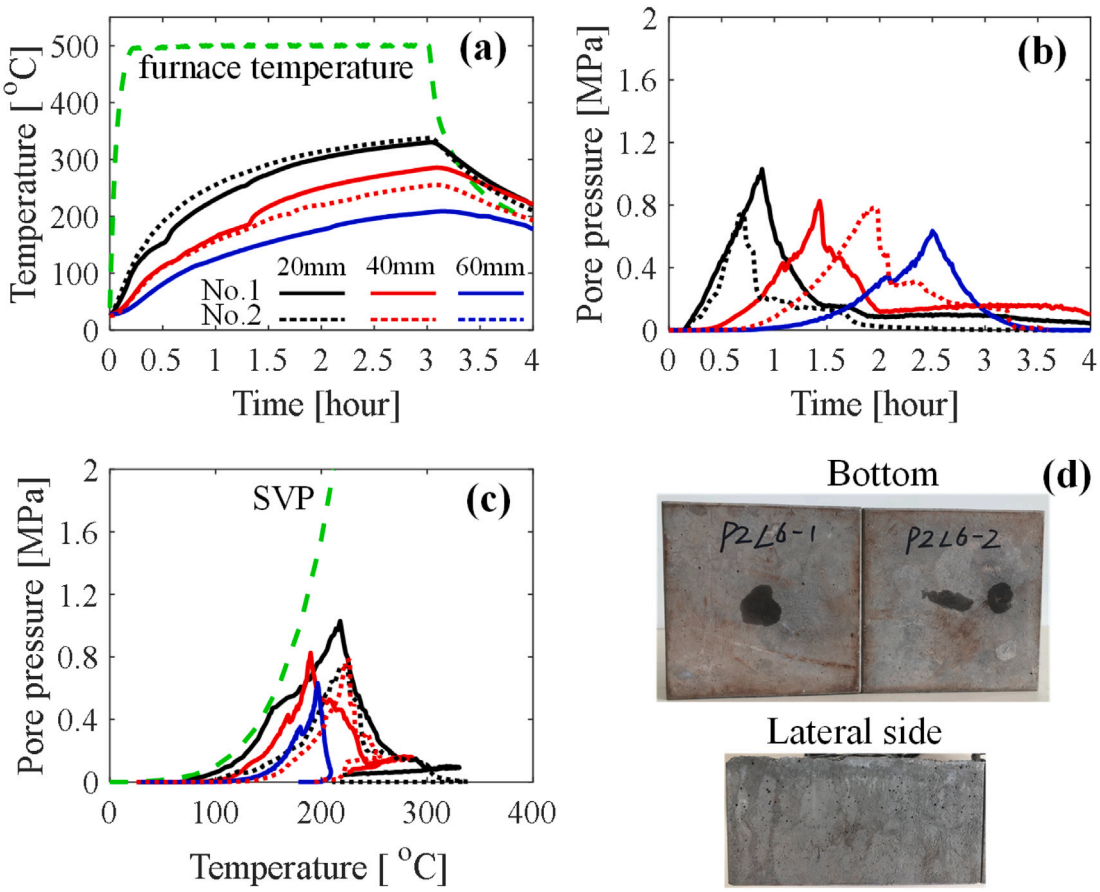

Fig. 10. Temperatures and pore pressures measured in S0P2L6: (a) temperature vs. time; (b) pore pressure vs. time; (a) pore pressure vs. temperature; (d) specimens after the thermal loading.

or even a local peak at the temperature of about 165 °C at a depth of 40 mm in the samples S1P2L12-1, S1P2L12-2, S2P2L12-1 and S2P4L12-2, and at 60 mm depth in specimens S1P2L12-1 and S2P4L12-2. To provide a clear comparison, the pore pressure versus temperature curves at a 60-mm depth of the different mixes, plain cementitious material, SFRC, PFRC and HFRC, are plotted together in Fig. 16(b). It can be observed clearly that the addition of steel fibers induces an increase in the pore pressure peak which decreases significantly when the fine PP fibers are added in the mix. Considering the HRFC mixes, the addition of fine PP fibers leads to a development of pore pressure under heating which is lower than that of plain cementitious material, S0P0, but higher than that of PFRC, S0P4L12, see Fig. 16(b). More importantly, as highlighted in the subplot of Fig. 16(b), a plateau occurs at the temperature of 165 °C which corresponds to the melting point of the PP fibers. This phenomenon clearly indicates that the effect of fine PP fibers on the pore pressure build-up acts significantly at the beginning of the melting process. However, the pressure that starts to build up from around 100 °C during heating, even before the PP fibers melt, can cause the poor PP fiber–matrix interfaces to break down resulting in the PITS in which the moisture vapor is able to expand resulting in a pressure relief [12,24,28,29]. This mechanism continues and enlarges even after the melting of PP fibers, in the temperature range of 165 °C–325 °C, in which the PP fibers exist as liquid phase that partially fills the tunnel-type voids. This process in combination to the FAE creates a better crack network [21,37,57,58], which generates effective pore pressure relief mechanisms inside the heated concrete, see in Fig. 16.

Comparing the pore pressure development between plain cementitious material and SFRC, the increasing effect of steel fiber addition is remarkable regarding the rising rate and peak value of the pore pressure. However, a plateau at the temperature range of 100 °C–150 °C is also observed, which reflects the formation of a moisture clog with a rapid pressure increase due to water evaporation, and simultaneously a pressure drop due to water condensation [5,47]. As for the PFRC, the diminishing effect of fine PP fibers on the pore pressure build-up is so remarkable that the plateau at 165 °C is no longer visible. For HFRC, the pore pressure plateaus at 165 °C is clearly visible and this phenomenon becomes more evident as the dosage of steel and fine PP fibers increases. The results of the presented study show that PP fibers provide a good pore pressure relief mechanism inside heated concrete resulting in maximum pressures taking longer to build up and occurring further deeper within the sample.

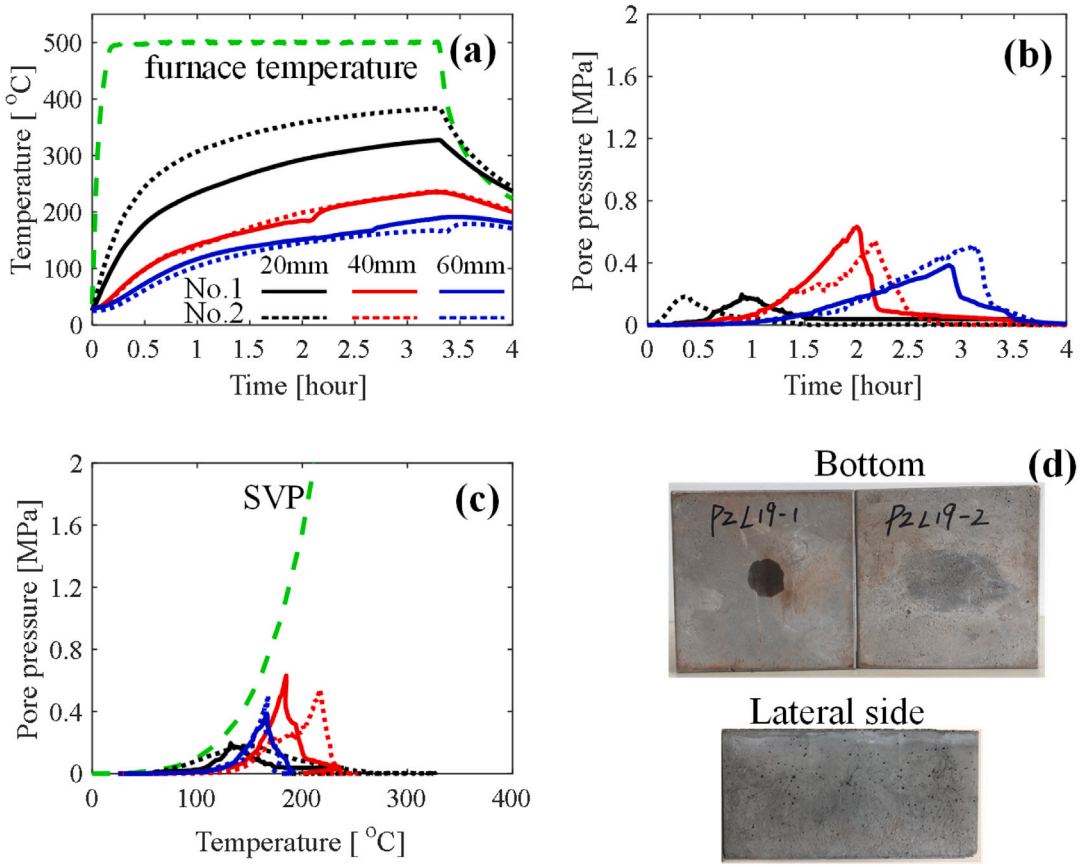

Fig. 11. Temperatures and pore pressures measured in S0P2L19: (a) temperature vs. time; (b) pore pressure vs. time; (a) pore pressure vs. temperature; (d) specimens after the thermal loading.

3.6. Effect of PP fiber length in HFRC

To investigate the influence of fine PP fiber length on pore pressure rise in samples of HFRC mixes, different mixtures with varying lengths of the PP fibers and fixed content (0.2% of PP fibers and 1% of steel fibers in volume) are employed and tested. Fig. 17 shows the experimental measurements for the mix S1P2L6 with PP fibers of 6 mm length, in which a maximum pressure of 1.88 MPa is observed at a depth of 20 mm, while the peaks of the pore pressure at deeper locations are about 1 MPa. Fig. 12 presents the results of the mix S1P2L12 with PP fibers of 12 mm length, in which the pore pressure reaches a maximum of 1.15 MPa at a depth of 40 mm and 60 mm. Fig. 18 reports the experimental data of the mix S1P2L19 with PP fibers of 19 mm length, in which the maximum pore pressure at each depth is about 0.5 MPa, apart from at a depth of 60 mm for the sample S1P2L19-1 where it is equal to 1 MPa. Although the pore pressure curves of the mix S1P2L6 and mix S1P2L19 are well captured, the pressure values vary significantly. This can be explained by the concrete heterogeneity, as it was numerically and experimentally studied in [47,65]. They showed that the relative position of sensors and coarse aggregates can significantly affect the pore pressure measurements. In addition, it is interesting to observe that the pressure variations appear over 150 °C, which may be caused by the random distribution of PP fibers. By comparing these peak values of the pore pressure it is clearly demonstrated that the increase in the length of fine PP fibers has a monotonous effect on the reduction of the pore pressure development employing a fixed fiber volume fraction, i.e. 0.2% of PP fibers and 1% of steel fibers. As reported in Table 2, the porosities of HFRCs decrease with the increase of fiber length after the heating treatment. These decrements of porosity are the result of the pore pressure relief due to the enhancement of the PITS mechanism and to the improvement of pore connectivity with longer PP fiber at high temperature. Furthermore, it is observed that maximum pore pressure occurs at a deeper position as the length of the PP fibers increases.

As discussed in the previous Section 3.4, the increasing length of fine PP fibers can increase particularly the FAE mechanism that favors the moisture diffusion and the pore pressure release. For the same reason, in HFRC, in addition to the thermal cracks caused by steel fiber thermal expansion, there are the mechanisms promoted by the fine PP fibers that synergistically increase the overall porosity of the material at elevated temperature mitigating the pore pressure rise inside concrete.

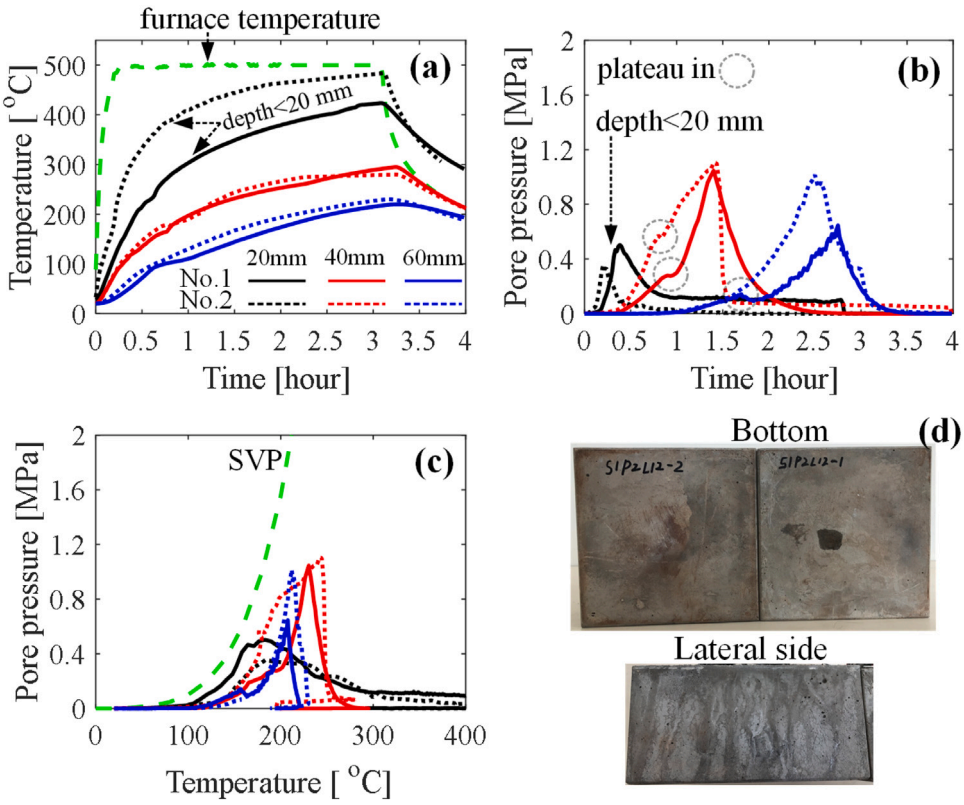

Fig. 12. Temperatures and pore pressures measured in S1P2L12: (a) temperature vs. time; (b) pore pressure vs. time; (a) pore pressure vs. temperature; (d) specimens after the thermal loading.

4. Discussion

4.1. Pore pressure and temperature

All the measured pore pressure peaks and the corresponding temperature are plotted in Fig. 19 with the isotherm straight line at 250 °C and SVP. The maximum pore pressure values and the corresponding temperature, depth, and time of pressure peaks for each mix are reported in Table 3. Most of the pore pressure peaks (96%) are within the temperature range of 150 °C–250 °C. The reference value is the pore pressure peak of the plain cementitious material (S0P0) with an average value of 1.2 MPa. Based on this value we have divided the results in 3 groups. The Group A collects the pressure peaks higher than the reference value and only the data of the mix S2P0 belong to this group. This occurrence suggests that only the addition of steel fibers is not recommended to improve the fire resistance of concrete structures, because the result is the opposite by increasing the spalling risk due to the higher pore pressure build-up. The experimental results of the mixes S1P0, S0P2L12, S0P2L6, S1P2L12, S1P2L6 and S2P02L12, belong to the Group B, which presents pore pressure peaks in the range between 60% and 100% of the reference value. The third Group C, which gathers the data of the mixes S0P2L19, S1P2L19, S0P4L12, S1P4L12 and S2P4L12, has the pore pressure peaks that range between 20% and 60% of the reference value. This result benefits from the improved permeability, as discussed previously, due to the addition of PP fibers. However, the addition of PP fibers alone is not recommended due to the excessive reduction of the residual mechanical strengths (see Table 2). Therefore, one should consider only the HFRC mixes of group C which retains the mechanical strength, i.e., mixes with steel fibers. Among the suitable HFRC mixes of group C, the best mix that meets the low spalling risk with a moderate price and sufficient workability is the S1P02L19, which also confirms the previous results in [26,27].

4.2. Comparison with experimental results in literature

Many experimental investigations on the measurement of pore pressure and temperature in concrete specimens exposed to elevated temperature are available in the literature; for a recent review one can look at [6]. In the literature different studies have developed most of the time different techniques for the pore pressure measurement which are differentiated by: the type of gage head, the filler adopted in the tube, the location of thermocouples, and the steel tube position, i.e. parallel or perpendicular to the heating surface. However, similar trends have been observed in different studies in which the major factors influencing pore pressure build-up at elevated temperature are:

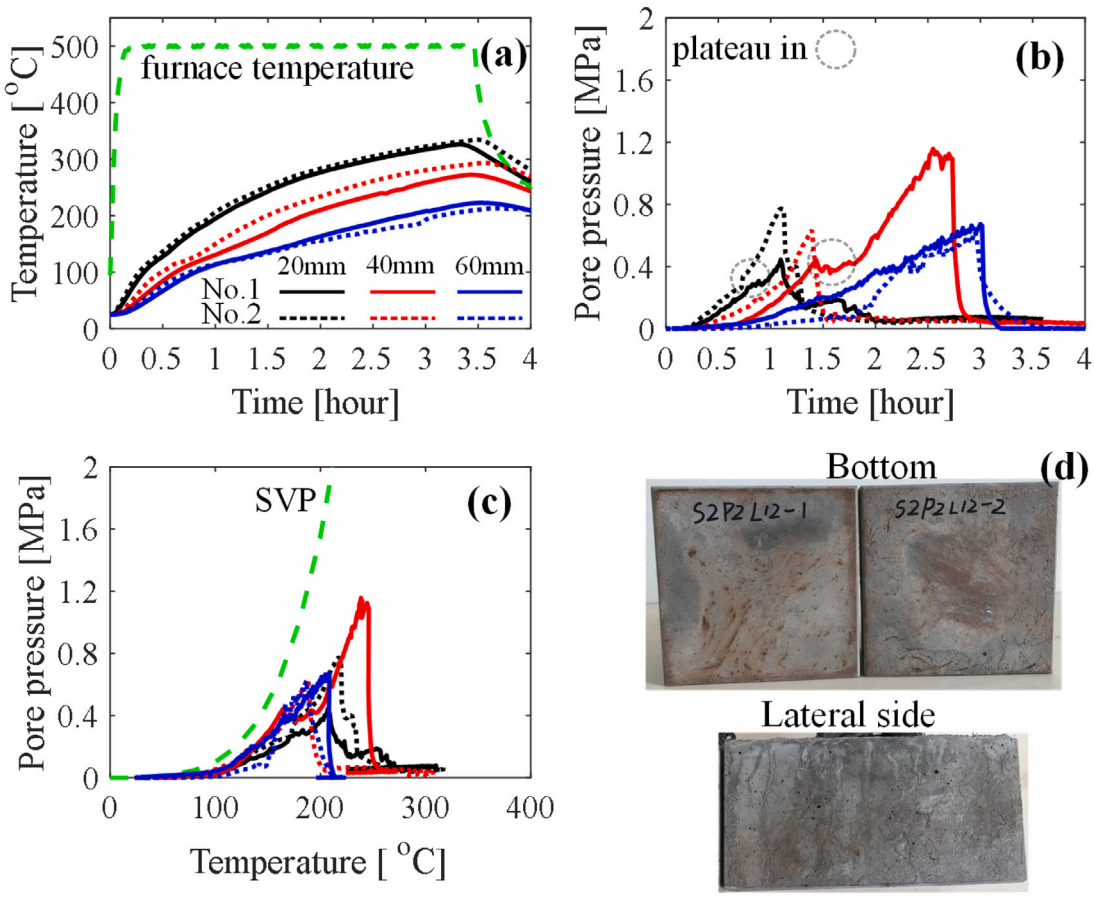

Fig. 13. Temperatures and pore pressures measured in S2P2L12: (a) temperature vs. time; (b) pore pressure vs. time; (a) pore pressure vs. temperature; (d) specimens after the thermal loading.

Table 3
Maximum pore pressure values for each mix.

Mix	Temp. at max pressure °C	Max pore pressure MPa	Time at max pressure hour	Depth of max pressure mm
S0P0	229.28	1.62	2.9	60
S1P0	223.56	1.17	0.82	20
S2P0	233.83	1.78	1.58	40
S0P2L12	304.88	0.68	0.95	20
S0P4L12	167.36	0.48	2.2	60
S0P2L6	217.74	0.99	0.88	20
S0P2L19	184.7	0.63	2	40
S1P2L12	241.72	1.1	1.4	40
S1P4L12	164.87	0.59	2.8	60
S2P2L12	238.53	1.16	2.55	40
S2P4L12	204.69	0.71	2.18	60
S1P2L6	240.6	1.83	0.87	20
S1P2L19	215.11	1.29	2.35	60

1. Microstructure and physical/mechanical properties (compressive strength, permeability, etc.). Many studies showed that concrete with higher strength is more prone to spall [48] since high strength concrete commonly presents a compact microstructure and low permeability that strongly influence pore pressure build-up under heating, see among others [10,27,66,67].
2. Effect of moisture content. The water content in concrete is strictly related to the pore pressure build-up at elevated temperature [68]. Typical experimental observations imply that the higher moisture content the larger the pore pressure development and the spalling risk [69–71].
3. Effect of heating rate. The increase of heating rate accelerates the pore pressure build-up closer to the exposed surface, boosting the spalling risk [72]. However, the effect of heating rate on the maximum value of the pore pressure is not fully clear

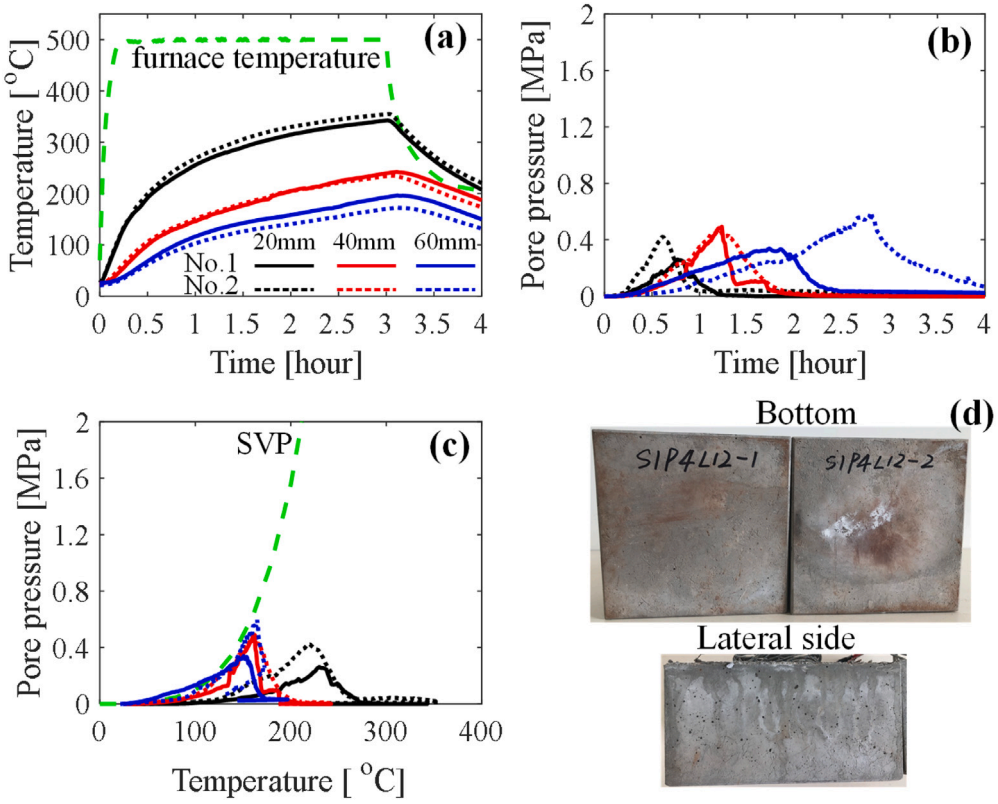

Fig. 14. Temperatures and pore pressures measured in S1P4L12: (a) temperature vs. time; (b) pore pressure vs. time; (a) pore pressure vs. temperature; (d) specimens after the thermal loading.

and seems to be reductive. As the matter of fact, the higher thermal gradient induces larger damage and more microcracks, which, in turn, generates higher permeability and facilitates water vapor releasing [67,70]. This process reduces significantly the pore pressure build-up.

4. Effect of lateral loading. Also the presence of lateral load has an effect on the pore pressure build-up and spalling risk [7,8]. When lateral loading is applied, the concrete spalling is facilitated, although the maximum pore pressure tends to reduce significantly. This is mainly due to the formation of damage and cracks generated by the compressive stresses in the direction parallel to the loading, which facilitate the pore pressure relief. On the contrary, when a limited biaxial loading is applied an increase of pore pressure is observed. This can be explained by the membrane compression stresses that prevent the crack formation in the heated surface and the water vapor from being released. Though increasing the biaxial compressive load more damage and cracks are generated in the concrete structure and this facilitate the pore pressure relief.
5. Effect of fibers. The use of PP fibers is the most widely adopted method to reduce the risk of explosive spalling at high temperature [24,35]. Many experimental investigations were performed on the cementitious composites with PP fibers [10,32,66,70]. The main mechanisms of the PP fibers in the pore pressure reduction has been discussed in the previous Sections 3.3 and 3.4. Also steel fibers have been used to reduce the spalling risk by resisting to the pore pressure build-up [73]. However, a more severe breaking-off of concrete could happen because of the higher pore pressure that has been observed [7,8]. Also other fiber types have been studied, although those are out of the scope of this research. For instance, the pore pressure development has been considered in the presence of jute and watersoluble PVA fibers [74]. Both of them have been effective in the reduction of the pore pressure peak, but not as effective as the PP fibers. The effect of PVA fibers was studied in [27] showing that the PVA fibers are less effective in mitigating pore pressure build-up than the PP fibers. In some studies also the synergistic effect of different types of fibers on reducing pore pressure build-up has been evaluated [26,75,76]. The mechanisms of different types of fibers with different melting points in the reduction of the pore-pressure build-up has been presented in 3.5. To summarize the results of different experimental investigations and the main influencing factors on the maximum pore pressure and corresponding temperature, the Table 4 has been created.

4.3. Prediction of relative maximum pressure

To provide a guidance for the anti-spalling mix design of cementitious material, a mathematical formula of the maximum pore pressure is proposed based on the experimental observations, which takes into account heating rate and some mix properties, such

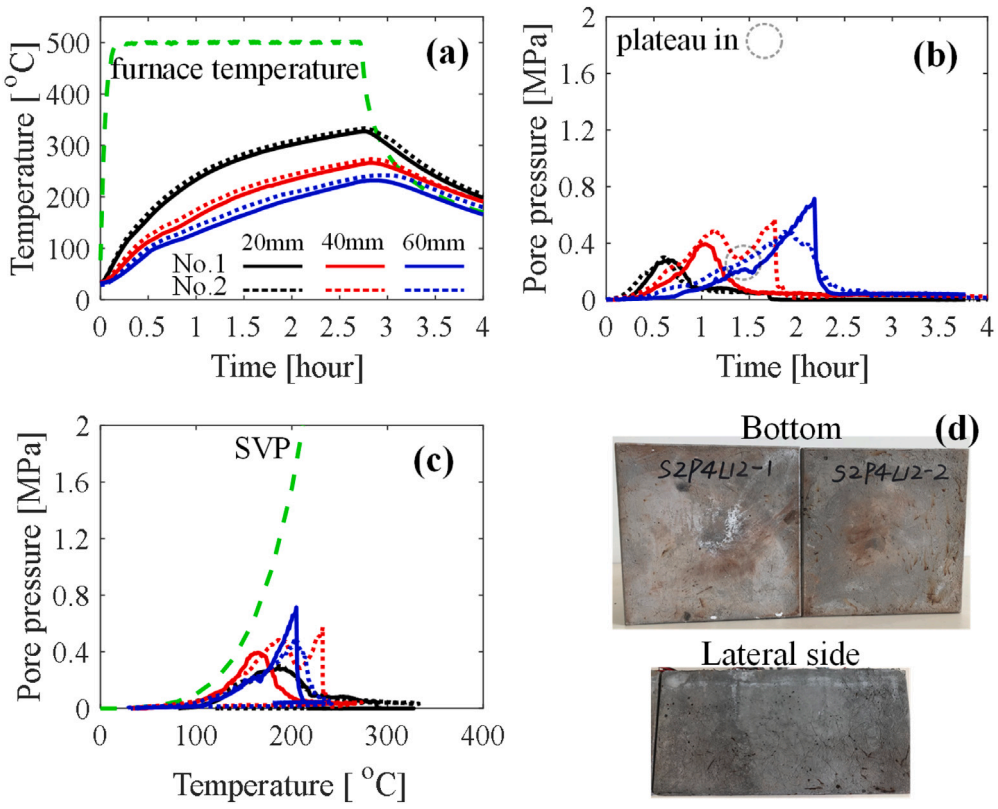

Fig. 15. Temperatures and pore pressures measured in S2P4L12: (a) temperature vs. time; (b) pore pressure vs. time; (a) pore pressure vs. temperature; (d) specimens after the thermal loading.

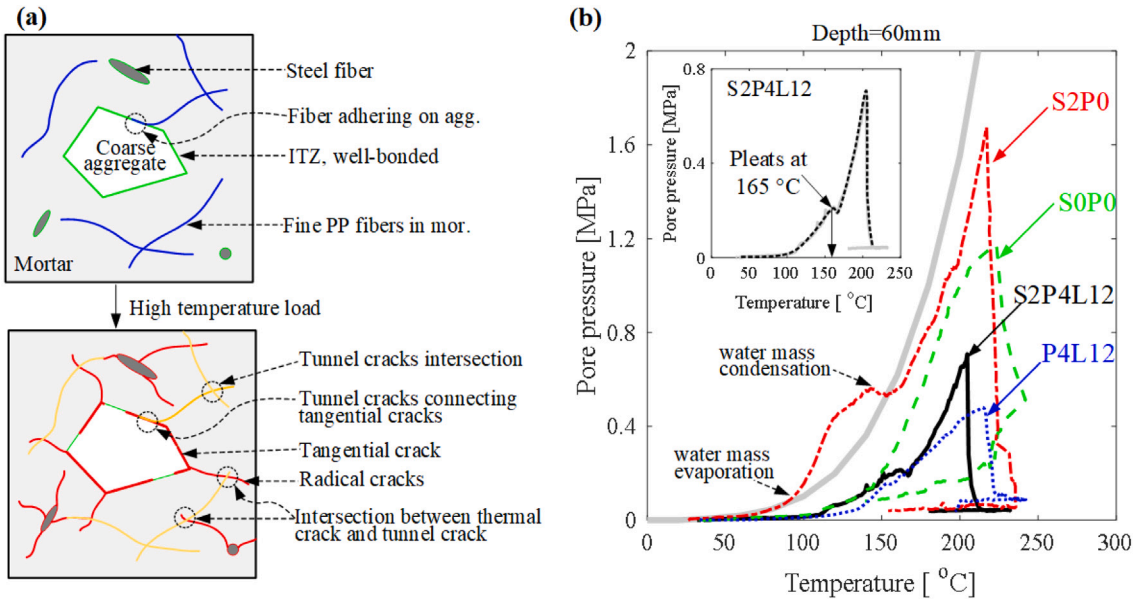

Fig. 16. Heating process in HFRC mixes: (a) the thermal damage distribution; (b) pore pressure vs temperature for different type of mixes at a depth of 60 mm from the heated surface.

as concrete strength, fiber type and fiber geometry. The relative pressure value is used instead of directly measured pore pressure to minimize the effects of measurement techniques and equipment errors used by different researchers, as well as the effects on

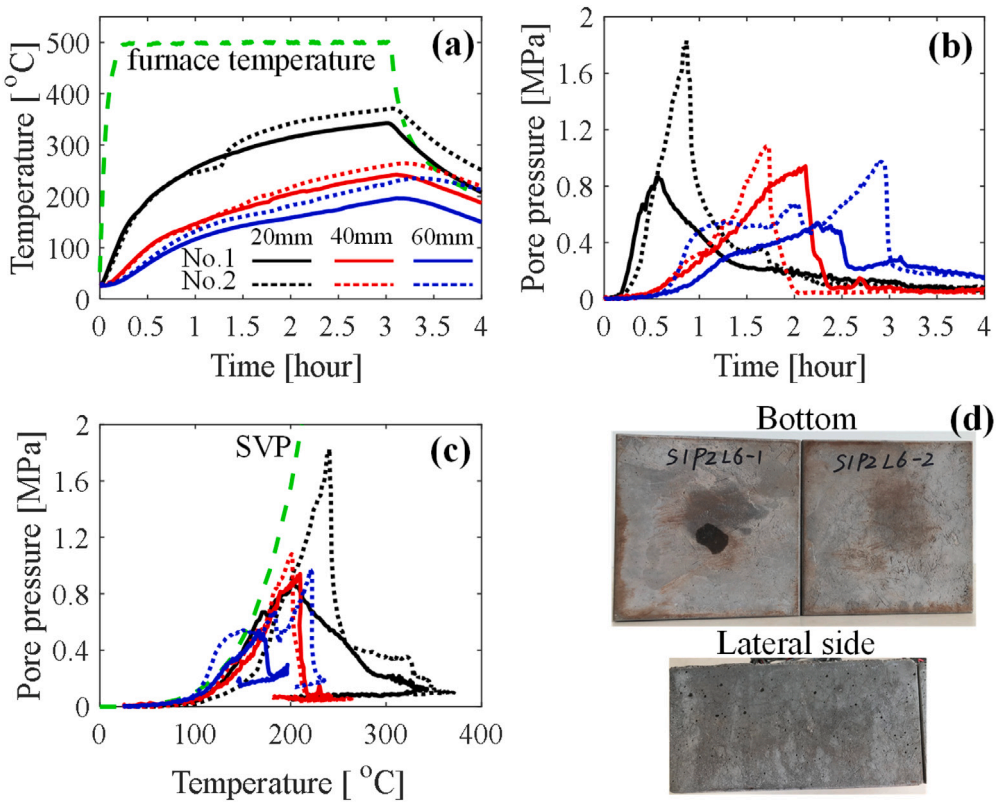

Fig. 17. Temperatures and pore pressures measured in S1P2L6: (a) temperature vs. time; (b) pore pressure vs. time; (a) pore pressure vs. temperature; (d) specimens after the thermal loading.

the composite properties, such as permeability, water content, etc. The relative maximum pressure, R_P, is obtained by dividing the measured maximum pressure, P_{max}^{mix}, by the maximum pressure measured for the reference plain cementitious material (matrix), P_{max}^{0}. The proposed formula reads

$$R_P = \frac{P_{max}^{mix}}{P_{max}^{0}} = \frac{f_c'^{\,mix}}{f_c'^{\,0}} - c_{s1} i_{SF} + c_{s2} \left(i_{SF}\right)^{c_{s3}} + c_{ps1} i_{PPF} i_{SF} + \left[c_{p1} A_{PPF} - c_{p2} \left(i_{PPF}\right)^{c_{p3}} + c_{p4} L_{PPF}\right] \cdot \exp\left(-c_{p5} \frac{T_{rate} - T_{rate}^{min}}{T_{rate}^{max} - T_{rate}^{min}}\right) \tag{1}$$

where, $f_c'^{\,mix}$ and $f_c'^{\,0}$ are the compressive strength of the considered mix and of the reference plain mix (without the fibers) at room temperature, respectively; A_{PPF} is the cumulative surface area of the PP fibers; i_{PPF} is the PP fiber index calculated as $i_{PPF} = V_{PPF} \cdot L_{PPF}/d_{PPF}$, in which V_{PPF} is the volume fraction of PP fibers, L_{PPF} is the length of PP fiber, and d_{PPF} is the diameter of PP fibers; $T_{rate}^{min} = 2$ °C/min and $T_{rate}^{max} = 120$ °C/min are the minimum and maximum temperature rate considered in the experiments; i_{SF} is the steel fiber index calculated as $i_{SF} = V_{SF} \cdot L_{SF}/d_{SF}$, in which V_{SF} is the volume fraction of steel fibers, L_{SF} is the length of steel fibers, and d_{SF} is the diameter of steel fibers; the c_i are the coefficients that need to be calibrated based on the experimental data. The law in Eq. (1), which predicts the relative maximum pressure when PP and/or steel fibers are added in the mix, is here termed ReMaPreF (RElative MAximum PREssure Formula). Note that the specimen size and shape do not affect the prediction of ReMaPreF since it considers only the ratio of strengths at room temperature, i.e. $f_c'^{\,mix}/f_c'^{\,0}$. The cooling methods can affect the residual strength of the thermally treated specimens. However, this effect is here neglected. Further studies on this effect are left for future studies. The fitting of experimental data in Tables 3 and 4 with the ReMaPreF law is here performed using the Levenberg–Marquardt nonlinear optimization, which gives the following values of the coefficients: $c_{p1} = 0.000241$, $c_{p2} = 0.8132$, $c_{p3} = 0.1933$, $c_{p4} = 5.433$, $c_{p5} = 0.4403$, $c_{s1} = 0.397$, $c_{s2} = 0.1$, $c_{s3} = 6.55$, $c_{ps1} = 0.0124$. For the sake of the mathematical statistics, eleven experimental campaigns with total 70 data points are adopted in the evaluation of the ReMaPreF coefficients. The ReMaPreF law gives quite good correlation between the numerical predictions and the experimental data. As shown in Fig. 20, ReMaPreF gives values of the square of the correlation, R^2, above 0.93 for all FRC. This result makes the aforementioned formula unique and reliable to quantitatively predict the effect of the fiber addition on the variation (reduction or increase) of the maximum pore pressure when the mix is exposed to high temperature.

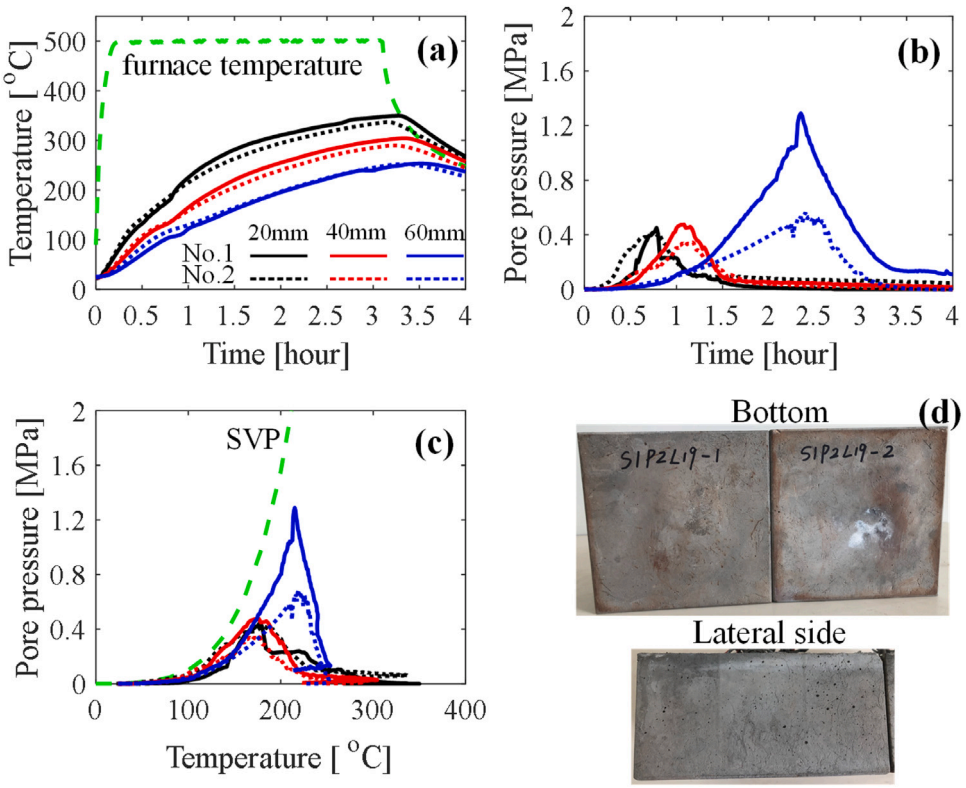

Fig. 18. Temperatures and pore pressures measured in S1P2L19: (a) temperature vs. time; (b) pore pressure vs. time; (a) pore pressure vs. temperature; (d) specimens after the thermal loading.

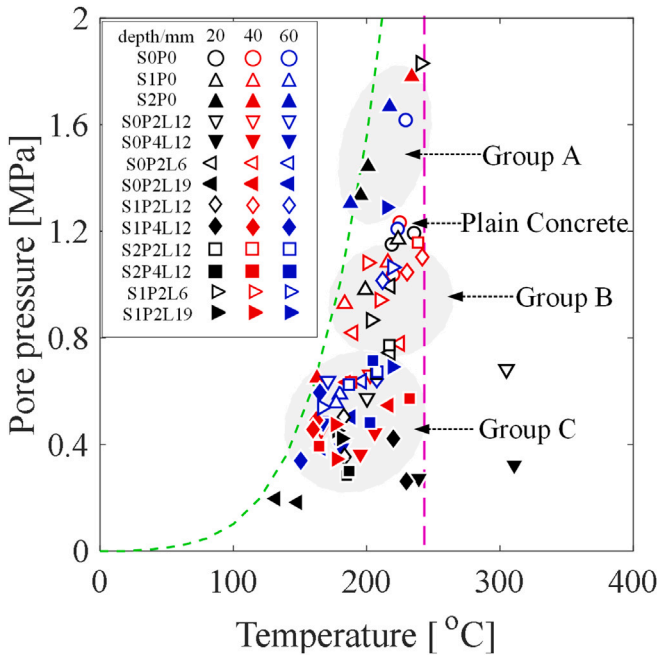

Fig. 19. Pore pressure peaks in the different mixes.

Table 4
Maximum pore pressure and corresponding temperature in literatures.

Mix	f'_c	d_{max}	PP fibers			Steel fibers			Temp. rate	Temp. max p	Max p	Ref.
	MPa	mm	d_{PPF} μm	L_{PPF} mm	V_{PPF} %	d_{SF} mm	L_{SF} mm	V_{SF} %	°C/min	°C	MPa	
Plain	111.6	20			0			0	5	252	4.0	[10]
PP-0.50	112.0	20	98	19	0.05			0	5	230	2.3	
PP-1.10	106.4	20	98	19	0.12			0	5	206	2.0	
PP-1.75	102.4	20	98	19	0.19			0	5	188	1.5	
PP-2.40	107.4	20	98	19	0.26			0	5	192	1.3	
PP-3.00	105.4	20	98	19	0.32			0	5	184	1.0	
Plain	89.7	13			0			0	10	290	5.0	[27]
PP 6–18	70.49	13	18	6	0.1			0	10	190	1.0	
PP 12–18	65.41	13	18	12	0.1			0	10	180	0.8	
PP 12–28	66.78	13	28	12	0.1			0	10	190	1.1	
HY(PP 6-18)	66.78	13	28	12	0.1	0.6 + 0.16	30 + 13	0.5	10	190	1.1	
Plain	93.08	13			0			0	5	Not available	4.0	[26]
PP 6–18	75.13	13	18	6	0.1			0	5		0.94	
HY1	76.53	13	18	6	0.1	0.6	30	0.3	5		1.01	
HY2	89.46	13	18	6	0.1	0.6	30	0.5	5		1.14	
HY3	83.97	13	18	6	0.1	0.6 + 0.16	30 + 13	0.3	5		1.03	
HY4	92.19	13	18	6	0.1	0.6	30	0.4	5		0.99	
Plain	63.2	15			0			0	50	245	1.2	[77]
MicroPP	61.5	15	18	9	0.11			0	50	300	0.62	
S	65.3	15			0	0.63	60	0.63	50	200	1.05	
MacroPP	67.0	15	740	45	0.44			0	50	220	0.9	
MicroPP-S	63.8	15	18	9	0.11	0.51	60	0.51	50	220	0.51	
MacroPP-S	67.2	15	740	45	0.44	0.51	60	0.51	50	220	0.7	
MicroPP-MacroPP-S	62.2	15	18 + 740	9 + 45	0.11 + 0.44	0.51	60	0.51	50	220	0.55	
Plain	149.6	0.6			0			0	2	246	2.69	[11,36]
PP[a]	159.7	0.6	12	30	0.33			0	2	217	3.32	
ST	172.1	0.6			0	0.22	13	2.5	2	268	5.16	
PPST	154.8	0.6	12	30	0.33	0.22	13	2.5	2	222	2.77	
Plain	63.2	18			0			0	120	240	1.19	[75]
MicroPPF1	61.5	18	18	9	0.11			0	120	199	0.64	
SF50	65.3	18			0	0.75	60	0.64	120	197	1.02	
MacroPPF4	67.0	18	740	45	0.44			0	120	235	0.84	
SF40 + MicroPPF1	63.8	18	18	9	0.11	0.75	60	0.51	120	210	0.49	
SF40 + MacroPPF4	67.2	18	740	45	0.44	0.75	60	0.51	120	240	0.68	
SF40 + MicroPPF05 + MacroPPF2	62.2	15	18 + 740	9 + 45	0.11 + 0.44	0.75	60	0.51	120	242	0.56	
Plain 70S	62	16			0			0	120	200	0.69	[34]
70S PM2	60	16	20	12	0.22			0	120	200	0.29	
70S PF2	61	16	48	12	0.22			0	120	200	0.6	
70S SF40[a]	63					0.55	35	0.51	120	200	0.6	
Plain B40	37	20	18	12	0			0	2	Not available	1.1	[78]
PP	37	20	18	12	0.22			0	2		0.55	
PP	37	20	18	12	0.22			0	10		0.3	
Plain B40	37	20			0			0	120	Not available	1.5	[66]
B40F2	29	20	18	12	0.22			0	120		0.4	
Plain B40SC	43	20			0			0	120		0.7	
B40SCF2	46	20	18	12	0.22			0	120		0.4	
Plain B60	61	20			0			0	120		2.55	
B60F2	70	20	18	12	0.22			0	120		0.75	

[a]Datum not used in the model fitting.

The fibers with high or low melting point show opposite contribution to the pore pressure development depending also on their amount and geometry as pointed out in Section 4.1. The proposed ReMaPreF law is capable of capturing all those features. The comparison between predicted and measured R_P is displayed in Fig. 20. The influence of fiber type and geometry on maximum measured pore pressure in this study is in very good agreement with the data obtained by other researchers. It is worth noting that the ReMaPreF formula just needs the concrete compression strength, the mix composition, and the temperature rate of the heating process to predict the reduction or the increase of the pore pressure when two kinds of fibers, PP or/and steel, are employed. Comparing with linear regression equations in the literature [27,75], the proposed ReMaPreF presents some improvements: a new formula is proposed; the rate of heating load is here considered, which is a major factor proved by the relevant experimental studies (see in Table 4); a non-linear regression approach is adopted in the presented optimization; the ReMaPreF presents a better fitting of the experimental data with $R^2 > 0.9$ (no proposed formula achieves such measure of fitting goodness).

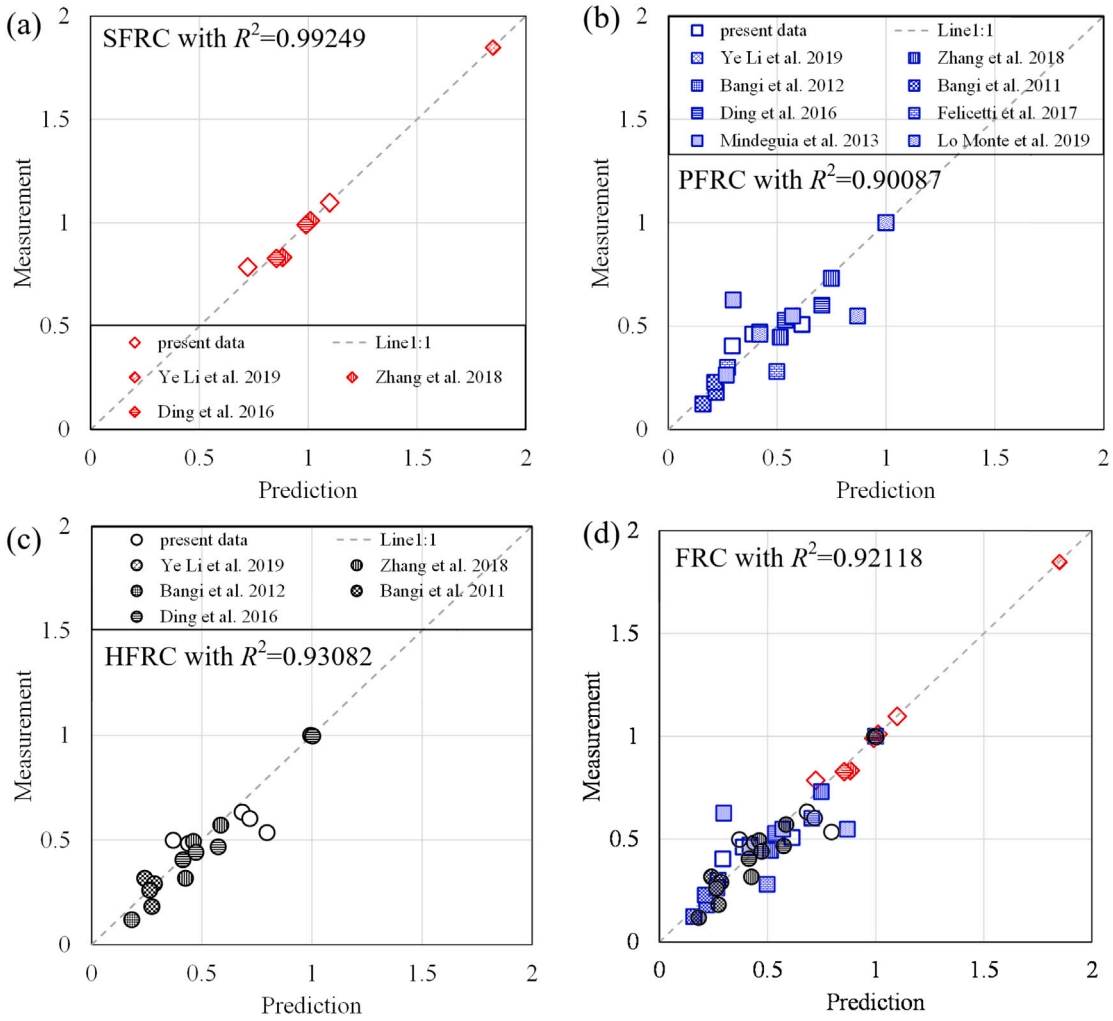

Fig. 20. Comparison between predicted and measured relative maximum pressure for fiber reinforced concrete: (a) SFRC, (b) PFRC, (c) HFRC, and (d) FRC.

5. Conclusions

The hybrid high and low melting point fiber-reinforced concrete (HFRC) is an effective solution to avoid thermal spalling risk at high temperature. The addition of steel fibers with high melting point acts on the thermal stress mechanism, and, at the same time, the addition of fine polypropylene (PP) fibers with low melting point acts on the pore pressure mechanism. To gain quantitative suggestions for mix design, the pore pressure build-up and residual strength of thirteen concrete mixes are tested. The main conclusions of the present experimental investigation can be drawn as follows:

(a) The addition of steel and fine PP fibers in HFRC makes them able to perform well under fire loading since the HFRC mix makes up for the shortcomings (lower strength of PFRC and higher spalling risk of SFRC) and inherits the advantages (higher strength of SFRC and lower spalling risk of PFRC) of a single-type fiber-reinforced concrete. Noteworthy in the experimental measurements of the pore pressure is observed in some HFRC mixes an evident plateau at 165 °C (PP melting temperature), which is the result of the synergistic effect of the two types of fibers.

(b) The increase of dosage and length of fine PP fibers causes a noticeable reduction of the maximum pore pressure. The increase of PP fiber length, rather than the dosage, is recommended to mitigate the pore pressure build-up. Because the dosage increase enlarges the porosity of matrix at high temperature resulting in lower residual strengths, while the length increase can develop a higher connectivity between pores and thermal cracks. Furthermore, the increase of fine PP fiber length can augment the probability of the fibers to adhere on coarse aggregates promoting the so-called “fiber adhering effect” (FAE). The FAE in combination with the mechanism of the pressure-induced tangential spaces (PITS) make the moisture vapor able to expand and escape resulting in a pressure relief.

(c) A new formula, termed ReMaPreF (RElative MAximum PREssure Formula), is proposed to predict the expected variation of the maximum pore pressure in different cementitious composites. The ReMaPreF takes into account the compression strength and heating rate, as well as the geometry, type and dosage of the adopted fibers.

In further research, the experimental data of this work will be used to develop an effective thermo-hygro-mechanical coupling model starting from Shen et al. [4,5] for HFRC at high temperature in order to extend the presented results on the maximum pore pressure considering various heating rate, fiber types, optimal fiber dimensions, specimen dimensional effect, and moisture content.

CRediT authorship contribution statement

Lei Shen: Conceptualization, Methodology, Experimental investigation, Validation, Writing – original draft, Writing – review & editing, Funding acquisition. **Xiupeng Yao:** Methodology, Experimental investigation, Validation, Writing – original draft. **Giovanni Di Luzio:** Methodology, Validation, Writing – original draft, Writing – review & editing. **Mingkai Jiang:** Experimental investigation. **Yang Han:** Experimental investigation.

Declaration of competing interest

The authors declare that they have no known competing financial interests or personal relationships that could have appeared to influence the work reported in this paper.

Data availability

Data will be made available on request.

Acknowledgments

This work was supported by the National Natural Science Foundation of China (51908195), and Fundamental Research Funds for the Central Universities, China (B220201030, B220204001). The authors would highly thank the efforts on the experiments from De Zhu (Henan University of Technology).

References

[1] D. Gawin, F. Pesavento, B. Schrefler, Towards prediction of the thermal spalling risk through a multi-phase porous media model of concrete, Comput. Methods Appl. Mech. Engrg. 195 (41) (2006) 5707–5729.
[2] J.-C. Liu, K.H. Tan, Y. Yao, A new perspective on nature of fire-induced spalling in concrete, Constr. Build. Mater. 184 (2018) 581–590.
[3] M. Ozawa, T. Tanibe, R. Kamata, Y. Uchida, K. Rokugo, S.S. Parajuli, Behavior of ring-restrained high-performance concrete under extreme heating and development of screening test, Constr. Build. Mater. 162 (2018) 215–228.
[4] L. Shen, W. Li, X. Zhou, J. Feng, G. Di Luzio, Q. Ren, G. Cusatis, Multiphysics lattice discrete particle model for the simulation of concrete thermal spalling, Cem. Concr. Compos. 106 (2020) 103457.
[5] L. Shen, F. Lo Monte, G. Di Luzio, G. Cusatis, Q. Ren, On the moisture migration of concrete subject to high temperature with different heating rates, Cem. Concr. Res. 146 (2021) 106492.
[6] Y. Li, E.-H. Yang, A. Zhou, T. Liu, Pore pressure build-up and explosive spalling in concrete at elevated temperature: A review, Constr. Build. Mater. 284 (2021) 122818.
[7] F. Lo Monte, R. Felicetti, Heated slabs under biaxial compressive loading: a test set-up for the assessment of concrete sensitivity to spalling, Mater. Struct. 50 (4) (2017) 192.
[8] F. Lo Monte, R. Felicetti, C. Rossino, Fire spalling sensitivity of high-performanceconcrete in heated slabs under biaxial compressive loading, Mater. Struct. 14 (1) (2019) 14.
[9] P. Kalifa, F.-D. Menneteau, D. Quenard, Spalling and pore pressure in HPC at high temperatures, Cem. Concr. Res. 30 (12) (2000) 1915–1927.
[10] P. Kalifa, G. Chéné, C. Gallé, High-temperature behaviour of HPC with polypropylene fibres: From spalling to microstructure, Cem. Concr. Res. 31 (10) (2001) 1487–1499.
[11] Y. Li, K.H. Tan, E.H. Yang, Synergistic effects of hybrid polypropylene and steel fibers on explosive spalling prevention of ultra-high performance concrete at elevated temperature, Cem. Concr. Compos. 96 (2019) 174–181.
[12] J.C. Mindeguia, H. Carre, P. Pimienta, C. La Borderie, Experimental discussion on the mechanisms behind the fire spalling of concrete, Fire Mater. 39 (7) (2015) 619–635.
[13] W. Khaliq, V. Kodur, Thermal and mechanical properties of fiber reinforced high performance self-consolidating concrete at elevated temperatures, Cem. Concr. Res. 41 (11) (2011) 1112–1122.
[14] H. Li, L. Gang, Tensile properties of hybrid fiber-reinforced reactive powder concrete after exposure to elevated temperatures, Int. J. Concr. Struct. Mater. 10 (1) (2016) 29–37.
[15] L. Shen, G. Di Luzio, D. Zhu, X. Yao, G. Cusatis, M. Cao, Y. Han, Y. Wang, Q. Ren, Mechanical responses of steel fiber-reinforced concrete after exposure to high temperature: Experiments and mesoscale discrete modeling, J. Eng. Mech. 147 (11) (2021) 04021084.
[16] H. Li, X. Hao, Q. Qiao, B. Zhang, H. Li, Thermal properties of hybrid fiber-reinforced reactive powder concrete at high temperature, J. Mater. Civ. Eng. 32 (3) (2020) 04020022.
[17] L. Shen, X. Yao, D. Zhu, N.F. Alkayem, Q. Ren, A thermal cracking pattern-based multiscale homogenization method for effective thermal conductivity of steel fiber reinforced concrete after high temperature, Int. J. Heat Mass Transfer 180 (10) (2021) 121732.
[18] T. Zhang, Y. Zhang, H. Zhu, Z. Yan, Characterizing the thermal properties of hybrid polypropylene-steel fiber reinforced concrete under heat exposure: Insights into fiber geometry and orientation distribution, Compos. Struct. 275 (2021) 114457.
[19] L. Biolzi, S. Cattaneo, G. Rosati, Evaluating residual properties of thermally damaged concrete, Cem. Concr. Compos. 30 (10) (2008) 907–916.
[20] S. Cattaneo, L. Biolzi, Assessment of thermal damage in hybrid fiber-reinforced concrete, J. Mater. Civ. Eng. 22 (9) (2010) 836–845.

[21] Y. Li, P. Pimient, N. Pinoteau, K.H. Tan, Effect of aggregate size and inclusion of polypropylene and steel fibers on explosive spalling and pore pressure in ultra-high-performance concrete (UHPC) at elevated temperature, Cem. Concr. Compos. 99 (2019) 62–71.
[22] F. Lo Monte, R. Felicetti, M.J. Miah, The influence of pore pressure on fracture behaviour of normal-strength and high-performance concretes at high temperature, Cem. Concr. Compos. 104 (2019) 103388.
[23] N. Algourdin, P. Pliya, A.-L. Beaucour, A. Simon, A. Noumowé, Influence of polypropylene and steel fibres on thermal spalling and physical-mechanical properties of concrete under different heating rates, Constr. Build. Mater. 259 (2020) 119690.
[24] G.A. Khoury, Polypropylene fibres in heated concrete. Part 2: Pressure relief mechanisms and modelling criteria, Mag. Concr. Res. 60 (3) (2008) 189–204.
[25] J. Komen, P. Vesa, Effects of high temperature on the pore structure and strength of plain and polypropylene fiber reinforced cement pastes, Fire Technol. 39 (2003).
[26] M.R. Bangi, T. Horiguchi, Pore pressure development in hybrid fibre-reinforced high strength concrete at elevated temperatures, Cem. Concr. Res. 41 (11) (2011) 1150–1156.
[27] M.R. Bangi, T. Horiguchi, Effect of fibre type and geometry on maximum pore pressures in fibre-reinforced high strength concrete at elevated temperatures, Cem. Concr. Res. 42 (2) (2012) 459–466.
[28] M. Ozawa, H. Morimoto, Effects of various fibres on high-temperature spalling in high-performance concrete, Constr. Build. Mater. 71 (2014) 83–92.
[29] F. Lo Monte, F. Lombardi, R. Felicetti, M. Lualdi, Ground-penetrating radar monitoring of concrete at high temperature, Constr. Build. Mater. 151 (2017) 881–888.
[30] Z. Dong, D. Aravind, K.H. Tan, On the mechanism of prevention of explosive spalling in ultra-high performance concrete with polymer fibers, Cem. Concr. Res. 113 (2018) 169–177.
[31] S.L. Suhaendi, T. Horiguchi, Effect of short fibers on residual permeability and mechanical properties of hybrid fibre reinforced high strength concrete after heat exposition, Cem. Concr. Res. 36 (9) (2006) 1672–1678.
[32] X. Liu, G. Ye, G. De Schutter, Y. Yuan, L. Taerwe, On the mechanism of polypropylene fibres in preventing fire spalling in self-compacting and high-performance cement paste, Cem. Concr. Res. 38 (4) (2008) 487–499.
[33] F. Lo Monte, R. Felicetti, Heated slabs under biaxial compressive loading: a test set-up for the assessment of concrete sensitivity to spalling, Mater. Struct. 50 (4) (2017) 192.
[34] F. Lo Monte, R. Felicetti, C. Rossino, Fire spalling sensitivity of high-performance concrete in heated slabs under biaxial compressive loading, Mater. Struct. 52 (2019) 14.
[35] G.A. Khoury, B. Willoughby, Polypropylene fibres in heated concrete. Part 1: Molecular structure and materials behaviour, Mag. Concr. Res. 60 (2) (2008) 125–136.
[36] Y. Li, K.H. Tan, E.H. Yang, Influence of aggregate size and inclusion of polypropylene and steel fibers on the hot permeability of ultra-high performance concrete (UHPC) at elevated temperature, Constr. Build. Mater. 169 (2018) 629–637.
[37] Y. Li, Y. Zhang, E.H. Yang, K.H. Tan, Effects of geometry and fraction of polypropylene fibers on permeability of ultra-high performance concrete after heat exposure, Cem. Concr. Res. 116 (2019) 168–178.
[38] Y. Li, E.H. Yang, K.H. Tan, Flexural behavior of ultra-high performance hybrid fiber reinforced concrete at the ambient and elevated temperature, Constr. Build. Mater. 250 (2020) 118487.
[39] D. Gawin, F. Pesavento, B.A. Schrefler, What physical phenomena can be neglected when modelling concrete at high temperature? A comparative study. Part 1: Physical phenomena and mathematical model, Int. J. Solids Struct. 48 (13) (2011) 1927–1944.
[40] G. Di Luzio, L. Biolzi, Assessing the residual fracture properties of thermally damaged high strength concrete, Mech. Mater. 64 (2013) 27–43.
[41] D. Dauti, S. Dal Pont, B. Weber, M. Briffaut, N. Toropovs, M. Wyrzykowski, G. Sciumé, Modeling concrete exposed to high temperature: Impact of dehydration and retention curves on moisture migration, Int. J. Numer. Anal. Methods Geomech. 42 (13) (2018) 1516–1530.
[42] V. Kodur, S. Banerji, Modeling the fire-induced spalling in concrete structures incorporating hydro-thermo-mechanical stresses, Cem. Concr. Compos. 117 (2021) 103902.
[43] P. Ren, X. Hou, V. Kodur, C. Ge, Y. Zhao, W. Zhou, Modeling the fire response of reactive powder concrete beams with due consideration to explosive spalling, Constr. Build. Mater. 301 (2021) 124094.
[44] C. Huang, G. Zhao, Introduction of technical specification for fiber reinforced concrete structures(CECS38:2004), Build. Struct. 35 (4) (2005) 74–79.
[45] J.-C. Mindeguia, P. Pimienta, A. Noumowé, M. Kanema, Temperature, pore pressure and mass variation of concrete subjected to high temperature—experimental and numerical discussion on spalling risk, Cem. Concr. Res. 40 (3) (2010) 477–487.
[46] Y. Li, D. Zhang, K.H. Tan, On measuring techniques of pore pressure in concrete at elevated temperature, Cem. Concr. Compos. 114 (2020) 103737.
[47] D. Dauti, A. Tengattini, S. Dal Pont, N. Toropovs, M. Briffaut, B. Weber, Analysis of moisture migration in concrete at high temperature through in-situ neutron tomography, Cem. Concr. Res. 111 (2018) 41–55.
[48] G. Khoury, Effect of fire on concrete and concrete structures, Prog. Struct. Eng. Mater. 2 (4) (2000) 429–447.
[49] L. Biolzi, G. Di Luzio, J.F. Labuz, Mechanical properties of photocatalytic white concrete subjected to high temperatures, Cem. Concr. Compos. 39 (2013) 73–81.
[50] M. Safiuddin, N. Hearn, Comparison of ASTM saturation techniques for measuring the permeable porosity of concrete, Cem. Concr. Res. 35 (5) (2005) 1008–1013.
[51] D. Gawin, F. Pesavento, B.A. Schrefler, What physical phenomena can be neglected when modelling concrete at high temperature? A comparative study. Part 2: Comparison between models, Int. J. Solids Struct. 48 (13) (2011) 1945–1961.
[52] S.-M. Yang, W.-Q. Tao, Heat Transfer Theory, High Education Press, 2006.
[53] G. Di Luzio, G. Muciaccia, L. Biolzi, Size effect in thermally damaged concrete, Int. J. Damage Mech. 19 (5) (2010) 631–656.
[54] B. Powierza, L. Stelzner, T. Oesch, C. Gollwitzer, F. Weise, G. Bruno, Water migration in one-side heated concrete: 4D in-situ CT monitoring of the Moisture-Clog-Effect, J. Nondestruct. Eval. 38 (1) (2019) 15.
[55] N. Toropovs, F. Lo Monte, M. Wyrzykowski, B. Weber, G. Sahmenko, P. Vontobel, R. Felicetti, P. Lura, Real-time measurements of temperature, pressure and moisture profiles in high-performance concrete exposed to high temperatures during neutron radiography imaging, Cem. Concr. Res. 68 (2015) 166–173.
[56] G. van der Heijden, R. van Bijnen, L. Pel, H. Huinink, Moisture transport in heated concrete, as studied by NMR, and its consequences for fire spalling, Cem. Concr. Res. 37 (6) (2007) 894–901.
[57] Y. Fu, Y. Wong, C. Tang, C. Poon, Thermal induced stress and associated cracking in cement-based composite at elevated temperatures—-Part I: Thermal cracking around single inclusion, Cem. Concr. Compos. 26 (2) (2004) 99–111, Fire Resistance.
[58] Y. Fu, Y. Wong, C. Tang, C. Poon, Thermal induced stress and associated cracking in cement-based composite at elevated temperatures—-Part II: thermal cracking around multiple inclusions, Cem. Concr. Compos. 26 (2) (2004) 113–126, Fire Resistance.
[59] K.L. Scrivener, A.K. Crumbie, P. Laugesen, The interfacial transition zone (ITZ) between cement paste and aggregate in concrete, Interface Sci. 12 (4) (2004) 411–421.
[60] J. He, D. Lei, W. Xu, In-situ measurement of nominal compressive elastic modulus of interfacial transition zone in concrete by SEM-DIC coupled method, Cem. Concr. Compos. 114 (2020) 103779.
[61] J. He, D. Lei, G. Di Luzio, F. Zhu, P. Bai, Mechanical properties measurement and micro-damage characterization of ITZ in concrete by SEM-DIC method, Opt. Lasers Eng. 155 (2022) 107064.
[62] G. Di Luzio, G. Cusatis, Hygro-thermo-chemical modeling of high performance concrete. I: Theory, Cem. Concr. Compos. 31 (5) (2009) 301–308.

[63] G. Di Luzio, G. Cusatis, Hygro-thermo-chemical modeling of high performance concrete. II: Numerical implementation, calibration, and validation, Cem. Concr. Compos. 31 (5) (2009) 309–324.
[64] D. Bentz, Fibers, percolation, and spalling of high performance concrete, ACI Mater. J. 97 (3) (2000) 351–359.
[65] D. Dauti, S. Dal Pont, M. Briffaut, B. Weber, Modeling of 3D moisture distribution in heated concrete: From continuum towards mesoscopic approach, Int. J. Heat Mass Transfer 134 (2019) 1137–1152.
[66] M. Jean-Christophe, P. Pierre, H. Carre, L.B. Christian, Experimental analysis of concrete spalling due to fire exposure, Eur. J. Environ. Civ. Eng. 17 (6) (2013) 453–466.
[67] G. Choe, G. Kim, M. Yoon, E. Hwang, J. Nam, N. Guncunski, Effect of moisture migration and water vapor pressure build-up with the heating rate on concrete spalling type, Cem. Concr. Res. 116 (2019) 1–10.
[68] S.Y.N. Chan, G.-F. Peng, M. Anson, Fire behavior of high-performance concrete made with silica fume at various moisture contents, ACI Mater. J. 96 (3) (1999) 405–409.
[69] W. Copier, The spalling of normal weight and lightweight concrete exposed to fire, in: ACI Symposium Publication, Vol. 80, 1983, pp. 219–236.
[70] L. Phan, Pore pressure and explosive spalling in concrete, Mater. Struct. 41 (2008) 1623–1632.
[71] G.-F. Peng, X.-J. Niu, Y.-J. Shang, D.-P. Zhang, X.-W. Chen, H. Ding, Combined curing as a novel approach to improve resistance of ultra-high performance concrete to explosive spalling under high temperature and its mechanical properties, Cem. Concr. Res. 109 (2018) 147–158.
[72] M. Dwaikat, V. Kodur, Hydrothermal model for predicting fire-induced spalling in concrete structural systems, Fire Saf. J. 44 (3) (2009) 425–434.
[73] V. Kodur, L. Phan, Critical factors governing the fire performance of high strength concrete systems, Fire Saf. J. 42 (6) (2007) 482–488, Structures in Fire.
[74] M. Ozawa, H. Morimoto, Effects of various fibres on high-temperature spalling in high-performance concrete, Constr. Build. Mater. 71 (2014) 83–92.
[75] Y. Ding, C. Zhang, M. Cao, Z. Yulin, C. Azevedo, Influence of different fibers on the change of pore pressure of self-consolidating concrete exposed to fire, Constr. Build. Mater. 113 (2016) 456–469.
[76] Y. Li, P. Pimienta, N. Pinoteau, K.H. Tan, Effect of aggregate size and inclusion of polypropylene and steel fibers on explosive spalling and pore pressure in ultra-high-performance concrete (UHPC) at elevated temperature, Cem. Concr. Compos. 99 (2019) 62–71.
[77] C. Zhang, J.-C. Liu, S. Han, Y. Hua, Pore pressure and spalling in fire-exposed high-strength self-consolidating concrete reinforced with hybrid fibres, Eur. J. Environ. Civ. Eng. 25 (2018) 1–31.
[78] R. Felicetti, F. Lo Monte, P. Pimienta, A new test method to study the influence of pore pressure on fracture behaviour of concrete during heating, Cem. Concr. Res. 94 (2017) 13–23.